iScience

CellPress
OPEN ACCESS

Article

Activation of GDNF-ERK-Runx1 signaling contributes to P2X3R gene transcription and bone cancer pain

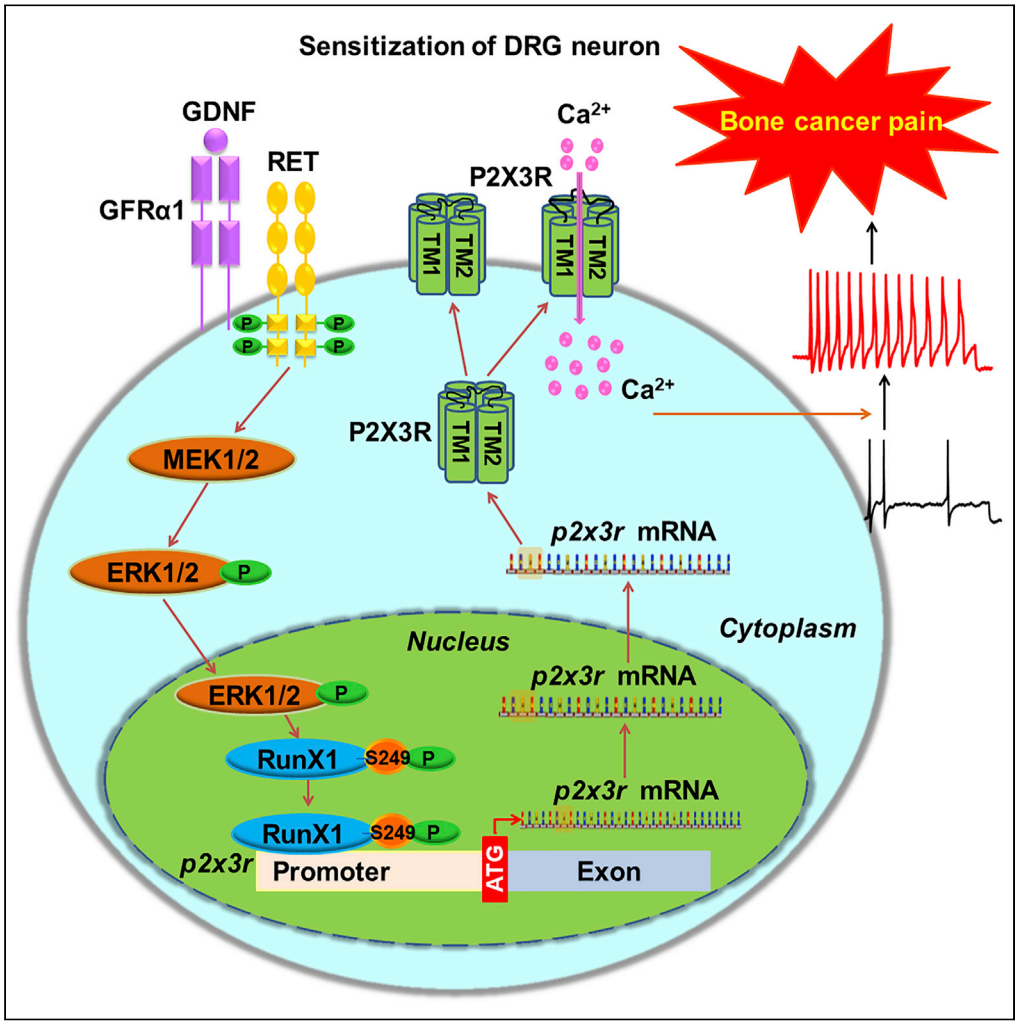

Zhu-Lin Yuan, Xiao-Dan Liu, Zi-Xian Zhang, ..., Xiao-Mei Yang, Min Liu, Guo-Gang Xing

ggxing@bjmu.edu.cn

Highlights

Runx1 directly upregulates the transcriptional activity of P2X3R gene promoter

Upregulation of Runx1-mediated P2X3R gene transcription underlies bone cancer pain

Involvement of GDNF-Ret-ERK signaling in Runx1-mediated P2X3R gene transcription

Yuan et al., iScience 25, 104936
September 16, 2022
https://doi.org/10.1016/j.isci.2022.104936

iScience

CellPress
OPEN ACCESS

Article

Activation of GDNF-ERK-Runx1 signaling contributes to P2X3R gene transcription and bone cancer pain

Zhu-Lin Yuan,[1,2,3,6] Xiao-Dan Liu,[1,2,3,6] Zi-Xian Zhang,[1,2,3,6] Song Li,[1,2,3] Yue Tian,[1,2,3] Ke Xi,[1,2,3] Jie Cai,[1,2,3] Xiao-Mei Yang,[4] Min Liu,[1,2,3,5] and Guo-Gang Xing[1,2,3,7,*]

SUMMARY

Bone cancer pain is a common symptom in cancer patients with bone metastases and its underlying mechanisms remain unknown. Here, we report that Runx1 directly upregulates the transcriptional activity of P2X3 receptor (P2X3R) gene promoter in PC12 cells. Knocking down Runx1 in dorsal root ganglion (DRG) neurons suppresses the functional upregulation of P2X3R, attenuates neuronal hyperexcitability and pain hypersensitivity in tumor-bearing rats, whereas overexpressing Runx1 promotes P2X3R gene transcription in DRG neurons, induces neuronal hyperexcitability and pain hypersensitivity in naïve rats. Activation of GDNF-GFRα1-Ret-ERK signaling is required for Runx1-mediated P2X3R gene transcription in DRG neurons, and contributes to neuronal hyperexcitability and pain hypersensitivity in tumor-bearing rats. These findings indicate that the Runx1-mediated P2X3R gene transcription resulted from activation of GDNF-GFRα1-Ret-ERK signaling contributes to the sensitization of DRG neurons and pathogenesis of bone cancer pain. Our findings identify a potentially targetable mechanism that may cause bone metastasis-associated pain in cancer patients.

INTRODUCTION

Bone cancer pain resulting from primary bone tumors or bone metastases is one of the most severe and intractable types of chronic pain (Andriessen et al., 2021). Understanding the mechanisms that cause it can inform drug development that may improve quality of life in patients. We and others have previously shown that the functional upregulation of P2X3 receptor (P2X3R) in dorsal root ganglion (DRG) contributes to the hyperexcitability of nociceptive sensory neurons and the pathogenesis of bone cancer pain (He et al., 2020b; Liu et al., 2013; Wu et al., 2012). However, the molecular mechanism underlying the transcriptional regulation of P2X3R in DRG neurons remains largely unknown.

Runx1, a Runt domain transcription factor, controlling the differentiation of nociceptors that express the neurotrophin receptor Ret, regulates the expression of many ion channels and receptors in DRG neurons, including ATP-gated P2X3R (Chen et al., 2006; Ugarte et al., 2012), therefore regulating several pain responses, including inflammatory pain and neuropathic pain (Abdel Samad et al., 2010; Chen et al., 2006; Kobayashi et al., 2012; Kramer et al., 2006; Marmigère et al., 2006; Yoshikawa et al., 2007). Mice lacking Runx1 exhibit specific defects in pain sensation (Chen et al., 2006), whereas postnatal activation of Runx1 increases the sensitivity to neuropathic pain (Kanaykina et al., 2010). In addition, Ret-deficient mice show a decreased expression of P2X3R mRNA in isolectin B4 $(IB4)^{+}$-DRG neurons, indicating an important role for Ret in the modulation of P2X3R gene transcription (Franck et al., 2011). It has been shown that Runx1 can bind to and directly upregulate the P2X3R gene promoter activity, thereby promoting the P2X3R gene transcription in various abnormal conditions (Nunez-Badinez et al., 2018; Ugarte et al., 2012). Moreover, post-translational modifications, especially the phosphorylated modification of Runx1 by activating mitogen-activated protein kinase (MAPK)/extracellular signal-regulated kinase (ERK) signaling (Bae and Lee, 2006; Hamelin et al., 2006; Ito, 1999; Kanno et al., 1998), affects the stabilization and transcriptional activity of Runx1 itself (Chuang et al., 2016; Goyama et al., 2015; Ito et al., 2015; Lie et al., 2020), raising the possibility that activation of MAPK/ERK signaling is required for phosphorylated modification of Runx1 and Runx1-mediated P3X3R transcription.

Glial cell line-derived neurotrophic factor (GDNF) has been shown to signal through a multicomponent receptor complex consisting of the Ret receptor tyrosine kinase and a member of the GFRα family of

[1]Neuroscience Research Institute, Peking University, Beijing 100191, China

[2]Department of Neurobiology, School of Basic Medical Sciences, Peking University Health Science Center, Beijing 100191, China

[3]Key Laboratory for Neuroscience, Ministry of Education of China and National Health Commission of China, Beijing 100191, China

[4]Department of Human Anatomy and Embryology, School of Basic Medical Sciences, Peking University, Beijing 100191, China

[5]Present address: Department of Physiology and Cardiovascular Research Institute, University of California, San Francisco, San Francisco, CA 94158, USA

[6]These authors contributed equally

[7]Lead contact

*Correspondence: ggxing@bjmu.edu.cn

https://doi.org/10.1016/j.isci.2022.104936

glycosyl-phosphatidylinositol-anchored receptors (Kawai and Takahashi, 2020; Takahashi, 2001). Serving as a receptor tyrosine kinase, Ret can activate various intracellular signaling pathways, including RAS/ERK, phosphatidylinositol 3-kinase (PI3K)/AKT, p38 MAPK and c-Jun N-terminal kinase (JNK) pathways (Hayashi et al., 2000; Kawai and Takahashi, 2020; Plaza-Menacho et al., 2006). Therefore, GDNF may serve as a potential contributor for the regulation of Runx1-mediated P2X3R gene transcription via the activation of GFRα-Ret-ERK signaling pathway. Also, GDNF has been shown to sensitize nociceptors and induce behavioral hyperalgesia in rodent models of chronic inflammatory pain (Malin et al., 2006) and muscle pain (Alvarez et al., 2012). Selective neurotoxic destruction of $IB4^+$ nociceptors or knockdown of GFRα1 by intrathecal antisense oligodeoxynucleotides to mRNA encoding GFRα1 attenuates both GDNF-induced hyperalgesia and the induction of chronic muscle pain (Alvarez et al., 2012). Intrathecal injection of lentivirus-mediated GDNF RNAi (LV-siGDNF) inhibits ERK activation in the spinal dorsal horn and alleviates mechanical and thermal hyperalgesia in a rat model of bone cancer pain (Meng et al., 2015).

In the present study, we explored the transcriptional regulation mechanism of P2X3R and its involvement in bone cancer pain. We uncovered that the Runx1-mediated P2X3R gene transcription via the activation of GDNF-GFRα1-Ret-ERK signaling contributes to the sensitization of DRG neurons and the pathogenesis of bone cancer pain. Our findings identify a potentially targetable mechanism that may cause bone metastasis-associated pain in cancer patients.

RESULTS

Upregulation of P2X3R and phosphorylated Runx1 in the DRG neurons of bone cancer rats, and enhancement of P2X3R gene promoter activity by Runx1 in PC12 cells

P2X3 receptors (P2X3R) are selectively expressed on primary afferent nociceptors and have been implicated in modulating nociception in various models of pathological pain (Bernier et al., 2018; Krajewski, 2020). Previously, we have reported that functional upregulation of P2X3R is involved in the pathogenesis of bone cancer pain, and pharmacological blockade of P2X3R has a significant analgesic effect on the bone cancer-induced mechanical allodynia and thermal hyperalgesia (Liu et al., 2013). In this study, we aimed to investigate the transcriptional regulation mechanism of P2X3R and its involvement in bone cancer pain. The rat model of bone cancer pain was developed by intratibial injections of MRMT-1 mammary gland carcinoma cells as described in our previous studies (Liu et al., 2013; Yang et al., 2018; Zheng et al., 2012, 2013). Radiographs showed extensive damage to the cortical bone and the trabeculae by day 14 after tumor cells inoculation, and by day 21, the damage was threatening the integrity of the tibial bone (Figure 1A). Significant pain hypersensitivity, including mechanical allodynia, thermal hyperalgesia, and spontaneous pain inferred respectively from the decreased paw withdrawal threshold (PWT) to mechanical stimuli (Figure 1B), the decreased paw withdrawal latency (PWL) to thermal stimulation (Figure 1C), and the increased number of flinching and the time spent guarding (Figures 1D and 1E), emerged in the ipsilateral hind paw of rats approximately at 10 to 14 days after tumor cells inoculation. In line with our previous findings, we indeed observed a significant upregulation of P2X3R expression in the ipsilateral L4/5 DRG neurons of tumor-bearing rats at 14 days after surgery, including an increase in P2X3R abundance at the mRNA (increased by ~66% versus PBS, *c*, $F_{(2,17)} = 30.15$, Figure 1F) and protein levels (increased by ~36% versus PBS, $p = 0.0031$, $F_{(2,9)} = 24.81$, Figure 1G). Moreover, the P2X3R was found to localize with Runx1 in the DRG neurons (Figures 1H–1L), and an enhanced immunofluorescence intensity was found both in P2X3R (increased by ~46% versus PBS, $p<0.0001$, $F_{(2,625)} = 304.3$, Figure 1K) and Runx1 (increased by ~47% versus PBS, $p<0.0001$, $F_{(21,079)} = 335.6$, Figure 1L) in cancer-bearing rat DRG neurons on day 14 after surgery. In addition, the phosphorylation level of Runx1 at serine 249 residue ($pRunx1^{Ser249}$) was increased in the ipsilateral L4/5 DRGs of bone cancer rats on day 14 after surgery (relative intensity of $pRunx1^{Ser249}$ ($pRunx1^{Ser249}$/Runx1): MRMT-1 1.54 ± 0.16 versus PBS 0.95 ± 0.03, $p = 0.0193$, $F_{(2,9)} = 11.99$, Figures 1M–1O). It is known that phosphorylated modification of Runx1 by activating MAPK/ERK signaling (Bae and Lee, 2006; Hamelin et al., 2006; Ito, 1999; Kanno et al., 1998) affects the stabilization and transcriptional activity of Runx1 itself (Chuang et al., 2016; Goyama et al., 2015; Ito et al., 2015; Lie et al., 2020). These results raise the possibility that the transcription factor Runx1 may serve as a regulator for P2X3R gene transcription.

To determine whether Runx1 can directly regulate P2X3R gene transcription, we performed transient transfection experiments using a construct carrying a 415 bp segment of the rat P2X3R gene promoter driving the expression of the Luciferase (Luc) reporter gene (p415-P2X3-Luc, Figure 1P, middle), and a plasmid coding for Runx1 (pcDNA3.1-Runx1) into the PC12 cells as described elsewhere (Ugarte et al., 2012). The

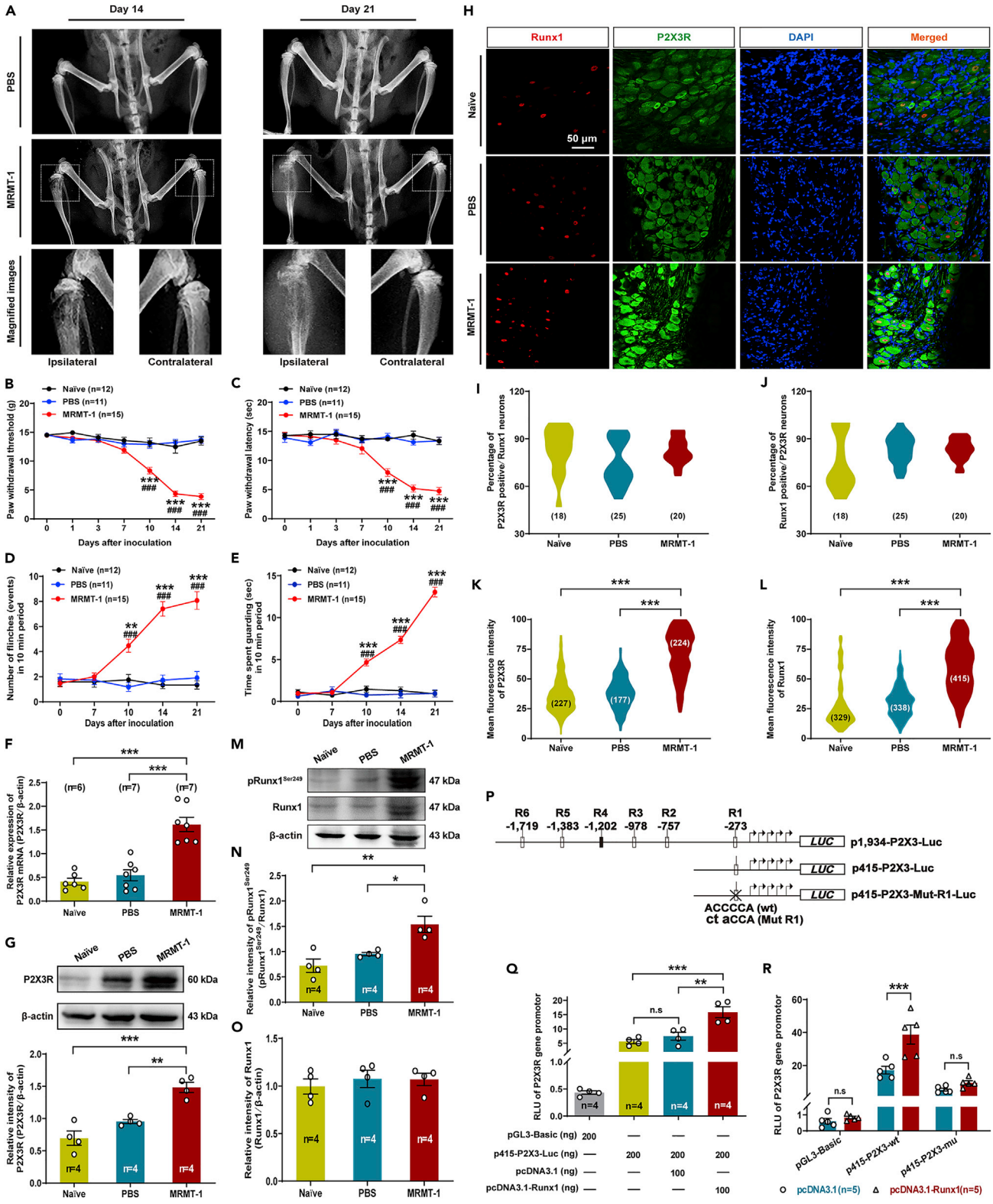

Figure 1. Upregulation of P2X3R gene promoter activity by Runx1

(A) Representative tibial bone radiographs obtained from PBS- and MRMT-1-treated rats on days 14 (left) and 21 (right) after surgery. The higher magnification of the proximal third of the bones from MRMT-1-treated rats (in the square box) are shown in the bottom. Note that severe deterioration with medullary bone loss and full-thickness bicortical bone loss were observed on ipsilateral but not contralateral tibia bone in MRMT-1-treated rats.

Figure 1. *Continued*

(B–E) Assessment of pain behaviors.

(B) Paw withdrawal threshold (PWT) in response to von Frey filaments stimuli.

(C) Paw withdrawal latency (PWL) in response to radiant heat stimulation.

(D and E) Spontaneous flinching (D) and guarding (E) behaviors were video recorded to assess spontaneous pain. n = 11–15 rats per group. **p<0.01, ***p<0.001, MRMT-1 versus naïve; $^{###}$p<0.001, MRMT-1 versus PBS, repeated-measures two-way ANOVA with Tukey's *post hoc* test.

(F and G) RT-qPCR and Western blot analyses of P2X3R mRNA (F, n = 6–7 rats per group) and protein (G, n = 4 rats per group) abundance in ipsilateral L4/5 DRGs from naïve, PBS-, and MRMT-1-treated rats at 14 days after surgery. Upper in (G): Representative blots are shown.

(H–L) Immunofluorescent staining with P2X3R and Runx1 in L4/5 DRG neurons obtained from naïve, PBS-, and MRMT-1-treated rats at 14 days after surgery (n = 3 rats per group).

(H) Representative images showing the immunostaining of Runx1 (red), P2X3R (green), and DAPI (blue). Right: merged images. Scale bar = 50 μm.

(I–L) Violin plots show the statistical analysis for the percentage of P2X3R-positive neurons on Runx1-positive neurons (I), Runx1-positive neurons on P2X3R-positive neurons (J), mean fluorescence intensity of P2X3R immunoreactivity (K) and Runx1 immunoreactivity (L).

(M–O) Western blot analyses of Runx1 and pRunx1^{Ser249} protein abundance in ipsilateral L4/5 DRGs from naïve, PBS-, and MRMT-1-treated rats at 14 days after surgery (n = 4 rats per group).

(M) Representative blots are shown.

(N and O) Bar graphs show the statistical analysis for the relative intensity of pRunx1^{Ser249} (N) Runx1(O) blots.

(P) Schematic representation of luciferase reporter constructs carrying either the full-length (1,934 bp) rat P2X3R gene promoter containing 6 putative consensus-binding sites (R1-R6) for Runx1 (p1,934-P2X3-Luc), 5′ deletion of this promoter containing R1 Runx1 motif (p415-P2X3-Luc), or promoter carrying mutated R1 Runx1 motif (p415-P2X3-Mut-R1-Luc).

(Q) Forced expression of Runx1 upregulates P2X3R gene promoter activity in PC12 cells (n = 4 biological replicates).

(R) Mutation of Runx1-binding site R1 blocks the upregulation of P2X3R gene promoter activity by Runx1 overexpression (n = 5 biological replicates). RLU, relative luciferase units. Data are presented as mean ± SEM. *p<0.05, **p<0.01, ***p<0.001, one-way ANOVA with Tukey's *post hoc* test for (F), (G), (I)–(L), (N), (O), and (Q); two-way ANOVA with Sidak's *post hoc* test for (R).

results revealed that forced expression of Runx1 in these cells significantly promoted P2X3R gene promoter activity (increased by ~53% versus p415-P2X3-Luc + pcDNA3.1, p = 0.0004, $F_{(3,12)}$ = 26.65, Figure 1Q), indicating that Runx1 may function as a positive regulator of P2X3R gene promoter. As the p415-P2X3-Luc plasmid only retains one Runx1-binding site (R1 site, Figure 1P, top), which is a key contributor to Runx1-enhanced P2X3R gene promoter activity (Ugarte et al., 2012), we then used it as a template to mutate this site by site-directed mutagenesis. Changes in three consensus nucleotides of the R1 site, which abolish the Runx1 binding, were produced (p415-P2X3-Mut-R1-Luc, Figure 1P, bottom). The results showed that mutation of Runx1-binding site R1 (p415-P2X3-mu) prevented the Runx1-mediated enhancement of P2X3R gene promoter activity (Figure 1R), further confirming the understanding that Runx1 directly promotes P2X3R gene promoter activity in PC12 cells.

Knockdown of Runx1 in DRG neurons inhibits P2X3R gene transcription and protein expression, and reduces neuronal hyperexcitability and pain hypersensitivity in bone cancer rats

Next, we investigated whether knockdown of Runx1 in DRG neurons could prevent the enhancement of P2X3R mRNA and protein abundance in the DRG neurons of bone cancer rats via the disruption of Runx1-mediated P2X3R gene transcription. Knocking down Runx1 in DRG neurons was performed by intrathecal administration of small interfering RNA (siRNA) targeting for Runx1 (Runx1 siRNA) to bone metastasis model rats once every two days for three times, on day 7 after tumor cells inoculation, and the DRG tissues were obtained on day 14 after tumor cells inoculation for Western blotting analysis or patch-clamp recording. The results showed that the abundance of Runx1 protein was significantly decreased in ipsilateral L4/5 DRGs of Runx1 siRNA-treated rats (reduced by ~48% relative to scramble siRNA, p = 0.0254, $t_{(4)}$ = 3.48, Figure 2A), validating that intrathecal Runx1 siRNA could effectively knock down Runx1 in the DRG neurons. Along with the knockdown of Runx1 in DRG neurons, the abundance of P2X3R mRNA and protein was significantly decreased in ipsilateral L4/5 DRGs in bone metastasis model rats treated with Runx1 siRNA (reduced by ~64 and ~33% versus scramble siRNA, p = 0.0021, $t_{(20)}$ = 3.53 for P2X3R mRNA, and p = 0.0002, $t_{(6)}$ = 8.06 for protein, respectively, Figures 2B and 2C). Also, the current density of P2X3R, evoked by the agonist α,β-meATP (20 μM for 3 s), was substantially reduced in small-diameter DRG neurons of MRMT-1 rats treated with Runx1 siRNA (in pA/pF, siRNA 22.51 ± 2.57 versus scramble 38.99 ± 4.55, p = 0.0022, $t_{(29)}$ = 3.37, Figure 2D); and the neuronal excitability, inferred from the action potential (AP) numbers was concomitantly and substantially decreased in tumor-bearing rats treated with Runx1 siRNA (in spikes/sec, siRNA 18.4 ± 2.02 versus scramble 25.0 ± 1.78, p = 0.0260, $t_{(29)}$ = 2.35, Figure 2E). Correspondingly, the behavioral tests showed that despite the fact that thermal hyperalgesia, as measured by the reduced PWL in response to radiant heat stimulation, was not altered, the mechanical

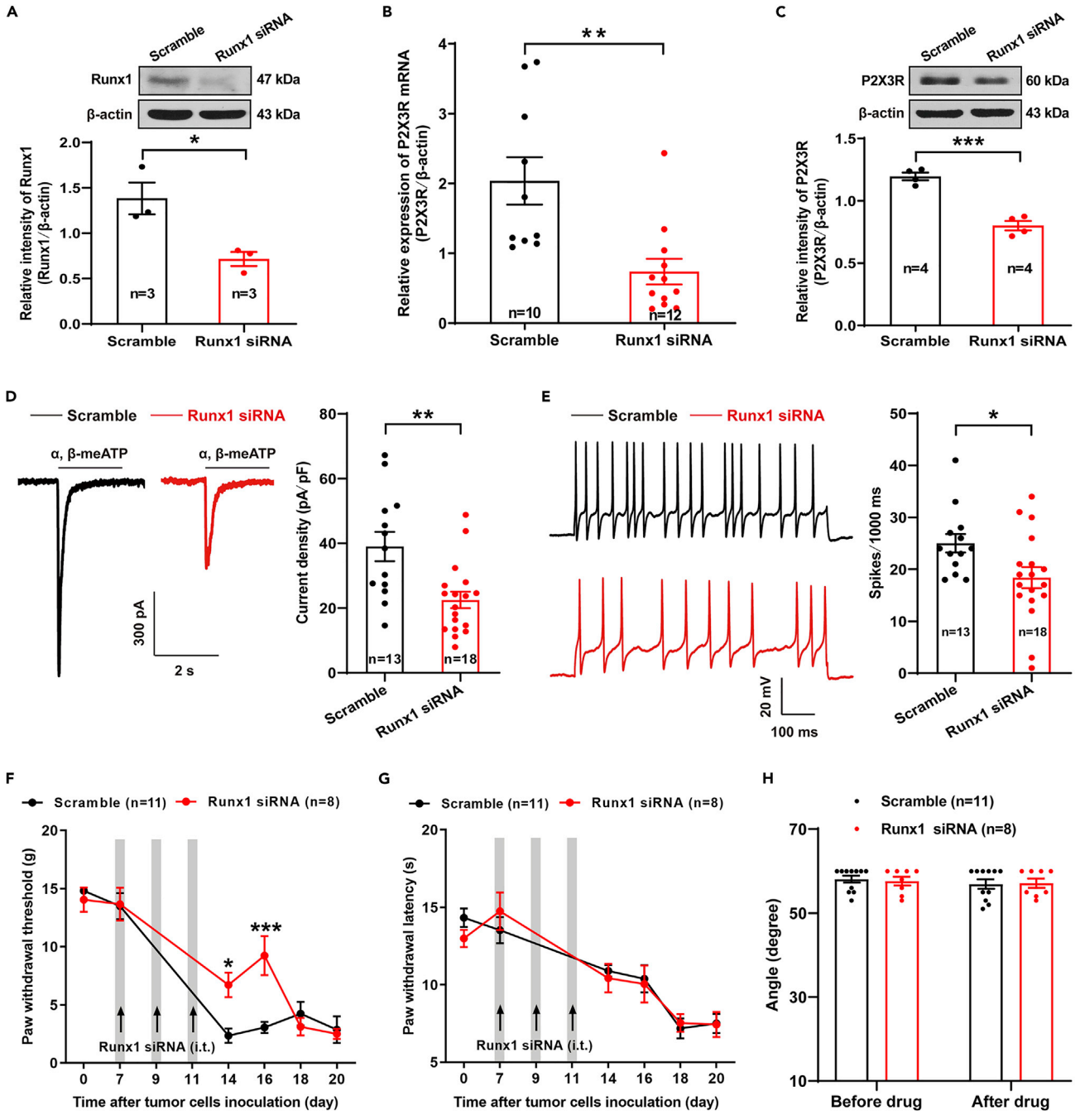

Figure 2. Runx1 knockdown reverses the increased P2X3R expression, DRG neurons hyperexcitability, and pain hypersensitivity in tumor–bearing rats

(A) Western blot analysis of Runx1 protein abundance in ipsilateral L4/5 DRGs from intrathecal scramble- and Runx1 siRNA-treated rats at 14 days after tumor cells inoculation (n = 3 rats per group). Upper: Representative blots are shown.

(B and C) RT-qPCR and Western blot analyses of P2X3R mRNA (B, n = 10–12 rats per group) and protein abundance (C, n = 4 rats per group) in ipsilateral L4/5 DRGs from intrathecal scramble- and Runx1 siRNA-treated rats at 14 days after tumor cells inoculation. Upper in (C): Representative blots are shown.

(D and E) Electrophysiological analyses of P2X3R currents (D) and neuronal excitability (E) in ipsilateral L4/5 DRG neurons from intrathecal scramble- and Runx1 siRNA-treated rats at 14 days after tumor cells inoculation (n = 12–18 cells from six to seven rats per group). Left in (D) and (E): Representative traces of α,β-meATP-induced P2X3R-currents (D) and neuronal action potentials (E) are shown.

Figure 2. *Continued*

(F and G) Assessment of ipsilateral PWT (F) and PWL (G) from intrathecal scramble- and Runx1 siRNA-treated rats from day 14 to day 20 after tumor cells inoculation (n = 8–11 rats per group).

(H) Assessment of animal's locomotor function by inclined-plate test, compared before and after drug administration (n = 8–11 rats per group). Data are presented as mean ± SEM. *p<0.05, **p<0.01, ***p<0.001, unpaired *t* test for (A)–(E); repeated-measures two-way ANOVA with Sidak's *post hoc* test for (F) and (G); two-way ANOVA with Sidak's *post hoc* test for (H).

hypersensitivity assessed by the decreased PWT in response to von Frey filaments stimuli was alleviated in bone cancer rats treated with Runx1 siRNA (on day 16 after tumor cells inoculation, siRNA 9.25 ± 1.69 g versus scramble 3.07 ± 0.48 g, p = 0.0001, $F_{(5,102)}$ = 4.89) (Figures 2F and 2G). Moreover, the results from inclined-plate test revealed that the animal's locomotor function was not impaired after intrathecal siRNA application (p = 0.9867, $F_{(1,34)}$ = 0.11, Figure 2H). These data indicate that knockdown of Runx1 in DRG neurons inhibits the P2X3R gene transcription and protein expression, subsequently reduces the neuronal hyperexcitability and pain hypersensitivity in bone cancer rats, supporting our understanding that the upregulation of Runx1-mediated P2X3R gene transcription is involved in the sensitization of DRG neurons and the pathogenesis of bone cancer pain.

Overexpression of Runx1 in DRG neurons promotes P2X3R gene transcription and protein expression, and enhances neuronal excitability and pain sensitivity in naïve rats

Furthermore, we explored whether overexpression of Runx1 in DRG neurons could promote P2X3R gene transcription and protein expression, and increase the neuronal excitability and pain sensitivity in naïve rats. Overexpression of Runx1 in DRG neurons was performed by intrathecal administration of lentivirus expressing Runx1 linked with GFP (LV-Runx1), and the DRG tissues were obtained at 14 days after virus injection for further immunostaining, Western blotting, real-time quantitative PCR (RT-qPCR), and patch-clamp recording, respectively. The results from immunofluorescence staining revealed that the mean immunofluorescence intensity of both Runx1 and P2X3R immunoreactivity was statistically increased in the DRG neurons of rats with LV-Runx1 treatment (increased by ~35 and ~46% relative to LV-GFP controls, p<0.0001, $t_{(264)}$ = 11.83 for Runx1, and p<0.0001, $t_{(175)}$ = 17.15 for P2X3R, respectively, Figures 3A–3C). Similar results were found in RT-qPCR and Western blotting analyses, showing that, relative to LV-GFP controls, the abundance of Runx1 protein, as well as P2X3R mRNA and protein were increased by ~35% (p = 0.0005, $t_{(6)}$ = 6.69), ~38% (p = 0.0122, $t_{(20)}$ = 2.76) and ~27% (p = 0.0058, $t_{(6)}$ = 4.18), respectively, in the DRGs of LV-Runx1-treated rats (Figures 3D–3F), indicating that intrathecal LV-Runx1 could effectively overexpress Runx1 in the DRG neurons, and subsequently promote the P2X3R gene transcription and protein expression in the DRG neurons of naïve rats. As a result, the P2X3R current in small-diameter DRG neurons (in pA/pF, LV-Runx1 25.30 ± 2.82 versus LV-GFP 12.22 ± 1.80, p = 0.0036, $t_{(12)}$ = 3.60, Figure 3G) and the neuronal excitability (in spikes/sec, LV-Runx1 8.33 ± 0.67 versus LV-GFP 4.82 ± 0.48, p = 0.0006, $t_{(24)}$ = 3.94, Figure 3H) were both increased substantially in LV-Runx1-treated rats compared with LV-GFP controls. The behavioral analysis showed that intrathecal LV-Runx1 produced a significant pain hypersensitivity, assessed by decreased PWT in response to von Frey filaments stimuli (p<0.0001, LV-Runx1 versus LV-GFP, from day 5 to day 21 after surgery, $F_{(10,261)}$ = 13.40, Figure 3I), although the PWL in response to radiant heat stimulation was not altered in rats treated with intrathecal LV-Runx1 (Figure 3J). Also, the inclined-plate test revealed that the animal's locomotor function was not impaired after intrathecal LV-Runx1 application (Figure 3K). These results suggest that overexpression of Runx1 in DRG neurons promotes P2X3R gene transcription and protein expression, thereby increasing the neuronal excitability and pain sensitivity in naïve rats.

Activation of ERK-dependent Runx1 phosphorylation and Runx1-mediated P2X3R gene transcription by GDNF

To further determine the upstream signaling molecules for the activation of Runx1-mediated P2X3R gene transcription in DRG neurons, we focused on GDNF, which has been shown to signal through a multicomponent receptor complex consisting of the Ret receptor tyrosine kinase and a member of the GFRα family of glycosyl-phosphatidylinositol-anchored receptors (Kawai and Takahashi, 2020; Takahashi, 2001). Binding of GDNF to GFRα1 induces Ret dimerization and autophosphorylation, subsequently activates various intracellular signaling cascades, including the RAS/ERK pathway (Costantini, 2010; Hayashi et al., 2000; Kawai and Takahashi, 2020; Kurtzeborn et al., 2019). Activation of ERK signaling is involved in the phosphorylated modification of Runx1, which affects the stabilization and transcriptional activity of Runx1 itself (Chuang et al., 2016; Goyama et al., 2015; Ito et al., 2015; Lie et al., 2020). Therefore, we speculated that activation of GDNF-GFRα1-Ret-ERK signaling cascades is likely required for Runx1-mediated P2X3R

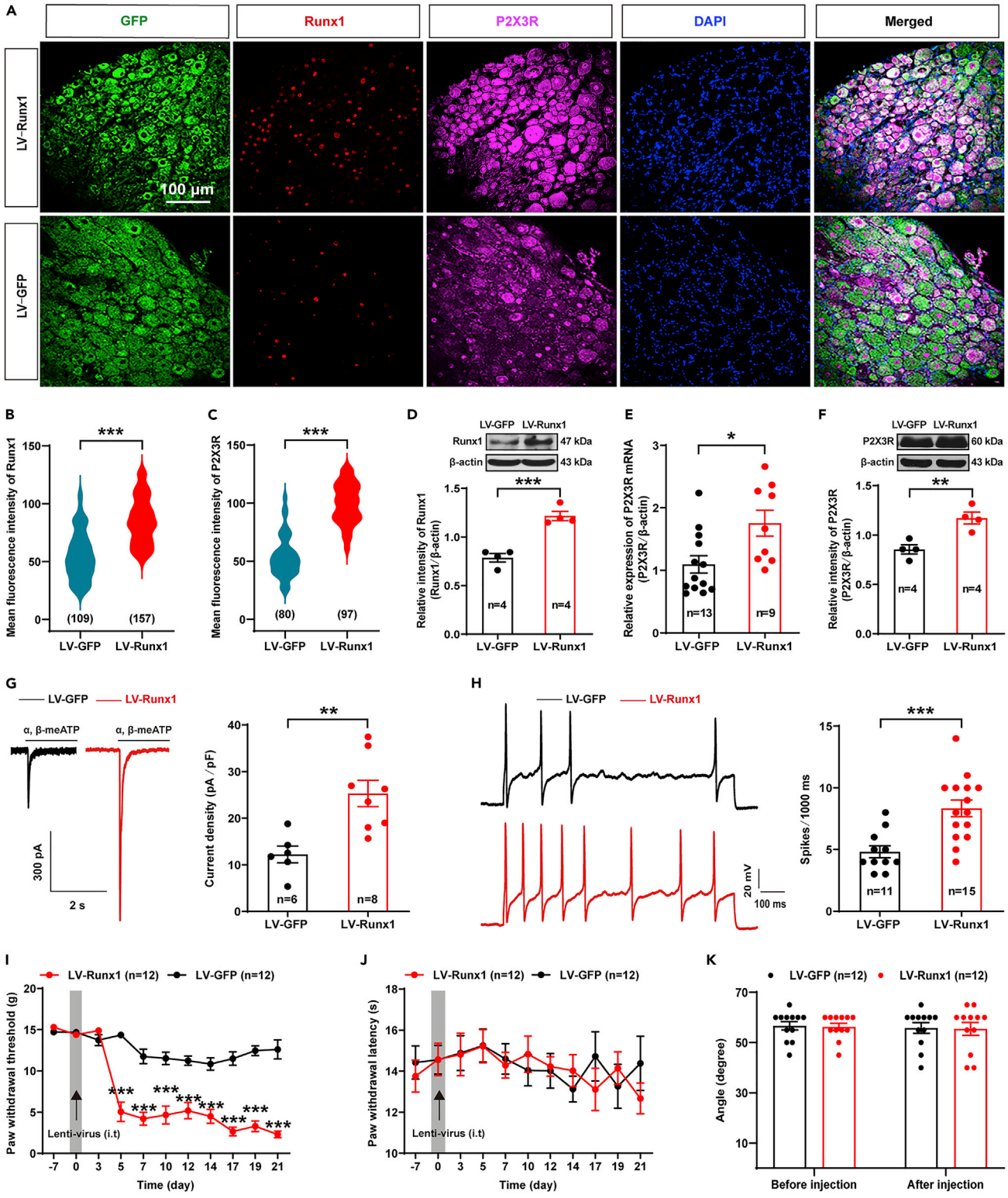

Figure 3. Runx1 overexpression induces the increases of P2X3R, DRG neurons hyperexcitability, and pain hypersensitivity in naïve rats

(A–C) Representative images (A) and a summary for the mean fluorescence intensity of Runx1 (B) and P2X3R (C) immunostaining in L4/5 DRG neurons from naïve rats at 14 days after intrathecal LV-Runx1 or LV-GFP administration (n = 80–157 cells from three rats per group). Scale bar = 100 μm.

Figure 3. *Continued*

(D) Western blot analysis of Runx1 protein abundance in L4/5 DRG neurons from naïve rats at 14 days after intrathecal LV-Runx1 or LV-GFP administration (n = 4 rats per group). Upper: Representative blots are shown.

(E and F) RT-qPCR and Western blot analyses of P2X3R mRNA (E, n = 9–13 rats per group) and protein (F, n = 4 rats per group) abundance in L4/5 DRGs from naïve rats at 14 days after intrathecal LV-Runx1 or LV-GFP administration. Upper in (F): Representative blots are shown.

(G and H) Electrophysiological analyses of P2X3R currents (G, n = 6–8 cells from five rats per group) and neuronal excitability (H, n = 11–15 cells from five rats per group) in L4/5 DRG neurons from naïve rats at 14 days after intrathecal LV-Runx1 or LV-GFP administration. Left in (G) and (H): Representative traces of α,β-meATP-induced P2X3R-currents (G) and neuronal action potentials (H) are shown.

(I and J) Assessment of PWT (I) and PWL (J) from naïve rats before and after intrathecal LV-Runx1 or LV-GFP administration (n = 12 rats per group).

(K) Assessment of animal's locomotor function before and after virus injection (n = 12 rats per group). Data are presented as mean ± SEM. *p<0.05, **p<0.01, ***p<0.001, unpaired *t* test for (B)–(H); repeated-measures two-way ANOVA with Sidak's *post hoc* test for (I) and (J); two-way ANOVA with Sidak's *post hoc* test for (K).

gene transcription in DRG neurons. To test this hypothesis, we first performed transient transfection experiments using SH-SY5Y human neuroblastoma cells that express endogenous GFRα1 and Ret (Fukuda et al., 2002), in which a construct carrying the full-length (1,934 bp) rat P2X3 gene promoter driving the expression of the luciferase reporter gene (p1,934-P2X3-Luc) with a plasmid coding for Runx1 (pcDNA3.1-Runx1 plasmids, Runx1-wt) (Figure 4A), or a plasmid of p1,934-P2X3-Luc with a plasmid coding mutated Runx1 at serine 249/266 sites (serine 249/266 sites were replaced with alanine or aspartic acid) (Figure 4B), were transfected into the SH-SY5Y cells. Then, the cells were respectively treated with recombinant human GDNF (100 ng/mL) for 24 h, or pretreated with PD98059 (20 μM, Merck Biosciences) for 30 min before GDNF (100 ng/mL) stimulation. The results showed that with the treatment of exogenous GDNF (100 ng/mL for 24 h), the P2X3R gene promoter activity was significantly increased, whereas pretreatment with PD98059, an inhibitor of MEK (the upstream kinase of ERK), significantly blocked this action of GDNF [in relative luciferase units (RLU), GDNF + DMSO 35.27 ± 2.31 versus GDNF + PD98059 15.02 ± 1.66, p = 0.0001, $F_{(2,12)}$ = 20.60, Figure 4A]. Meanwhile, with the treatment of exogenous GDNF also promoted the P2X3R gene promoter activity in SH-SY5Y cells co-expressing both P2X3R (p1,934-P2X3-Luc) and wild-type Runx1 (Runx1-wt) genes (in RLU, GDNF 58.20 ± 3.41 versus vehicle 42.29 ± 2.78, p = 0.0364, $F_{(2,18)}$ = 1.49), whereas this increased effect of GDNF was abolished by the mutation of Runx1 at serine 249/266 sites to alanine (S249/266A) or aspartic acid (S249/266D) (Figure 4B). These results indicate that GDNF likely promotes the Runx1-mediated P2X3R gene transcription by the activation of ERK signaling.

Then, we tested this understanding in cultured DRG neurons with exogenous GDNF (100 ng/mL) treatment. The results revealed that the P2X3R mRNA level was statistically increased (by ~52% relative to 0 h controls, p = 0.0002, $F_{(2,12)}$ = 23.31, Figure 4C) in cultured DRG neurons with 24 h GDNF treatment. Similarly, the abundance of both phosphorylated ERK (for 48 h, increased by ~36% relative to 0 h, p = 0.0011, $F_{(4,15)}$ = 7.93, Figures 4D–4F) and pRunx1^{Ser249} (for 48 h, increased by ~48% relative to 0 h, p = 0.0007, $F_{(4,15)}$ = 8.03, Figures 4G–4I) were substantially increased in cultured DRG neurons with GDNF treatment. Interestingly, the abundance of P2X3R protein displayed a bimodal increase, that is, the P2X3R protein abundance was increased at 6 h (by ~25%, relative to 0 h, p = 0.0143), fell down to the baseline at 12 h, raised again at 24 h, and lasted for 48 h (increased by ~36%, relative to 0 h, p = 0.0002) after GDNF treatment ($F_{(4,15)}$ = 10.32, Figures 4J and 4K). We speculated that a kind of rapid translational mechanism likely underlies the increase in P2X3R protein abundance at the early stage (6 h) because the level of P2X3R mRNA remained unchanged at this stage (Figure 4C), whereas both transcriptional and translational mechanisms are involved in the increased abundance of P2X3R protein at the late stage (24–48 h). In fact, we found that a protein translation inhibitor anisomycin could significantly block the GDNF-induced increase in P2X3R protein abundance (DMSO + GDNF 1.20 ± 0.04 versus anisomycin + GDNF 0.89 ± 0.10, p = 0.0122, $F_{(2,12)}$ = 7.55, Figure 4L) at the early stage (6 h).

To further test our understanding that the activation of GDNF-GFRα1-Ret-ERK signaling cascades is required for Runx1-mediated P2X3R gene transcription in DRG neurons, we first explored whether application of the GDNF antibody, the Ret inhibitor, or the downstream signaling molecules inhibitors, could respectively block the GDNF-induced activation of phosphorylated ERK and the upregulation of P2X3R mRNA and protein abundance in cultured DRG neurons. The results showed that both of the GDNF antibody and the Ret inhibitor (RPI-1) could significantly inhibit the GDNF-induced upregulation of phosphorylated ERK and P2X3R protein expression in cultured DRG neurons (Figures S1A–S1D). Next, because several signaling pathways including RAS/ERK, PI3K/AKT, p38 MAPK and JNK pathways are implicated as the intracellular signaling pathways activated by GDNF (Hayashi et al., 2000; Kawai and Takahashi,

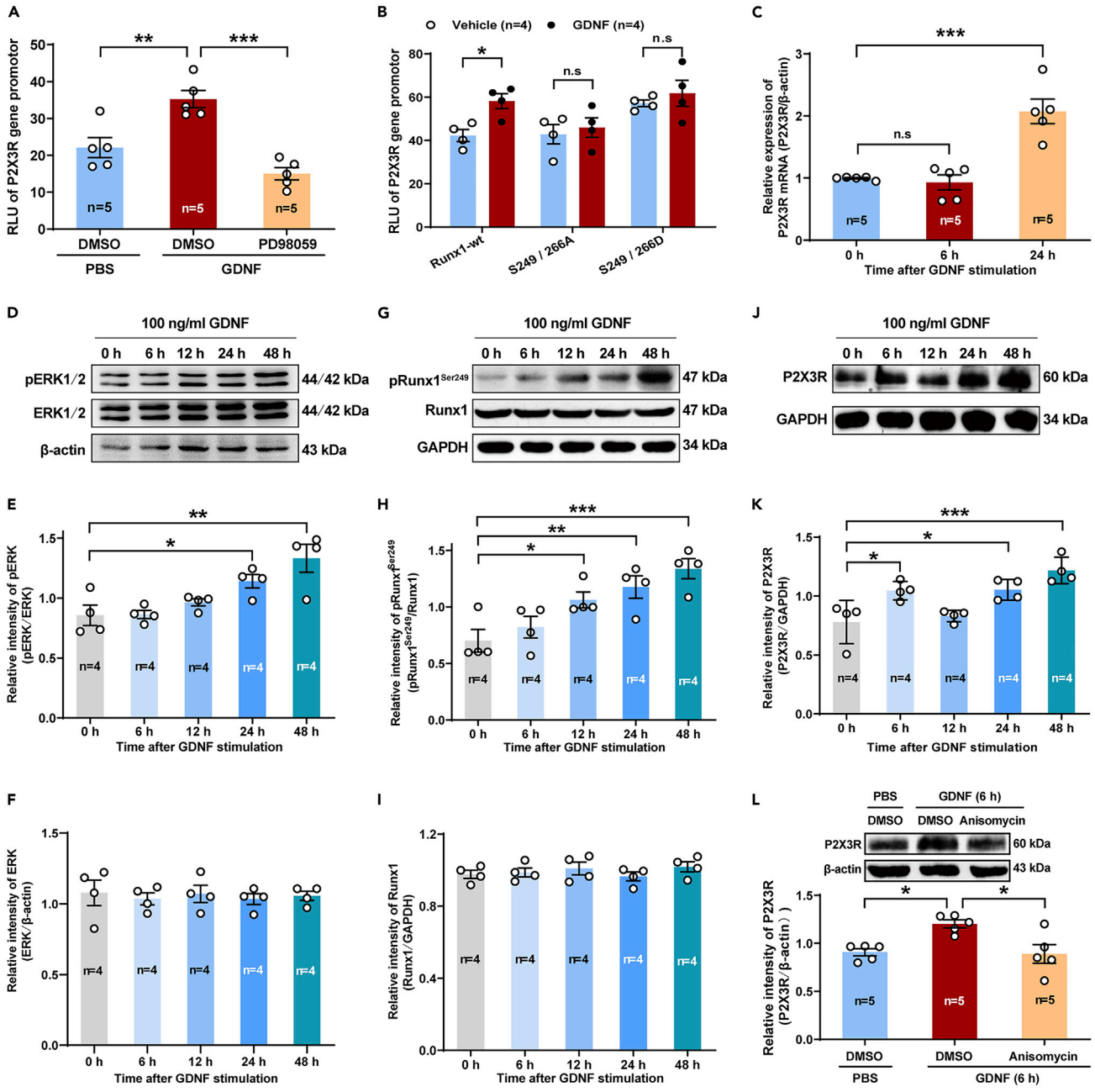

Figure 4. Exogenous GDNF upregulates P2X3R gene promoter activity in SH-SY5Y cells, increases the abundance of phosphorylated ERK, Runx1, and P2X3R mRNA and protein in cultured DRG neurons

(A) Luciferase reporter assay of P2X3R gene promoter activity in SH-SY5Y cells treated with GDNF or GDNF + PD98059.

(B) Mutation of Runx1 serine 249/266 sites blocks the increased P2X3R gene promoter activity by GDNF in SH-SY5Y cells. RLU, relative luciferase units.

(C) RT-qPCR analysis of P2X3R mRNA abundance in cultured DRG neurons with GDNF treatment.

(D–F) Western blot analysis of ERK and phosphorylated ERK abundance in cultured DRG neurons with GDNF treatment.

(D) Representative blots are shown.

(G–I) Western blot analysis of Runx1 and phosphorylated Runx1 abundance in cultured DRG neurons with GDNF treatment. (G) Representative blots are shown.

(J and K) Western blot analysis of P2X3R protein abundance in cultured DRG neurons with GDNF treatment.

(J) Representative blots are shown.

Figure 4. *Continued*

(L) Protein translation inhibitor, anisomycin, blocks the increased P2X3R protein abundance in cultured DRG neurons with 6 h GDNF treatment. (L) Representative blots are shown. n = 3–5 biological replicates per group as indicated. Data are presented as mean ± SEM. *p<0.05, **p<0.01, ***p<0.001, one-way ANOVA with Tukey's *post hoc* test for (A) and (L); two-way ANOVA with Sidak's *post hoc* test for (B); one-way ANOVA with Dunnett's *post hoc* test for (C), (E)–(F), and (H)–(I), and (K). See also Figure S1.

2020; Plaza-Menacho et al., 2006), we thus performed experiments to determine which signaling pathway is involved in Runx1-mediated P2X3R gene transcription activated by GDNF. The results revealed that the GDNF-induced increase of P2X3R protein abundance was significantly blocked by the MEK inhibitor PD98059, but not by the Src-family tyrosine kinases inhibitor PP2, or the PI3K inhibitor LY294002 (Figure S1E), indicating that the RAS/ERK signaling pathway is required for the GDNF-induced upregulation of P2X3R protein abundance. Indeed, we found that blocking the ERK signaling using PD98059 also prevented the GDNF-induced increase of P2X3R mRNA expression (reduced by ~58% relative to DMSO, p<0.0001, $F_{(2,12)}$ = 43.45, Figure S1F). Together these data with the aforementioned findings, we suggest that the activation of the ERK signaling is involved in Runx1-mediated P2X3R gene transcription activated by GDNF in cultured DRG neurons.

Intrathecal GDNF activates ERK-Runx1 signaling cascade, increases P2X3R gene transcription and neuronal excitability in DRG neurons, and induces pain hypersensitivity in naïve rats

Furthermore, we investigated the effects of intrathecal GDNF on the activation of ERK-Runx1 signaling cascade, as well as on P2X3R gene transcription, DRG neurons excitability, and pain sensitivity in naïve rats. Recombinant human GDNF (200 ng in a 10-μL volume) or vehicle was intrathecally administered to the naïve rats once per day for three consecutive days, and the following biochemical analysis, electrophysiological recording, and behavioral testing were respectively performed at one day after the last drug injection. In line with the aforementioned findings as shown in the *in vitro* cultured DRG neurons (Figures 4 and S1), we saw that the abundance of both phosphorylated ERK (increased by ~33% versus vehicle, p = 0.0056, $t_{(8)}$ = 3.76, Figure 5A) and phosphorylated Runx1 at serine 249 site (increased by ~54% versus vehicle, p = 0.0048, $t_{(6)}$ = 4.36, Figure 5B) were substantially increased in the DRG neurons of rats with intrathecal GDNF treatment. Meanwhile, the levels of both P2X3R mRNA (increased by ~63% versus vehicle, p = 0.0013, $t_{(10)}$ = 4.44, Figure 5C) and protein (increased by ~28% versus vehicle, p = 0.0004, $t_{(6)}$= 6.96, Figure 5D) abundance, as well as the α,β-meATP-induced P2X3R currents (increased by ~41% versus vehicle, p<0.0001, $t_{(23)}$ = 5.16, Figure 5E) and the neuronal excitability (AP numbers, increased by ~53% versus vehicle, p = 0.0002, $t_{(40)}$ = 4.11, Figure 5F) in small-diameter DRG neurons, were significantly increased in the intrathecal GDNF-treated rats. Moreover, the behavioral analysis showed that intrathecal administration of GDNF produced both mechanical hypersensitivity and thermal hyperalgesia in naïve rats inferred from decreased PWT and PWL in bilateral hind paws of GDNF-treated rats relative to controls (Figures 5G–5J). The results from inclined-plate test revealed that the animal's locomotor function was not impaired after intrathecal GDNF administration (Figure 5K).

In addition, we performed experiments to test whether pretreatment with ERK inhibitor (SCH772984) or Runx1 siRNA, could prevent the effects of intrathecal GDNF on P2X3R mRNA and protein expression and the pain sensitivity in naïve rats. In these experiments, SCH772984 (15 μM × 10 μL), or alternatively, Runx1 siRNA or scramble siRNA (2.5 μg in a 10-μL volume), was intrathecally administered to the naïve rats at 1 h before GDNF application. The results showed that the intrathecal GDNF-induced increase of $pRunx1^{Ser249}$ abundance in L4/5 DRGs was substantially inhibited by the ERK inhibitor SCH772984 (reduced by ~42% relative to vehicle, p = 0.0016, $t_{(10)}$ = 4.30, Figure S2A). Also, the increased levels of P2X3R mRNA and protein abundance in L4/5 DRGs, induced by intrathecal GDNF, were significantly restored by the pretreatment of ERK inhibitor SCH772984 (relative to vehicle, reduced by ~47 and ~32%, p = 0.0007, $t_{(12)}$ = 4.48 for P2X3R mRNA, and p = 0.0419, $t_{(6)}$ = 2.58 for P2X3R protein, respectively, Figures S2B and S2C). The behavioral studies showed that pretreatment with SCH772984 could effectively abrogate the intrathecal GDNF-induced pain hypersensitivity in naïve rats, as indicated by decreased PWT (after drug: SCH + GDNF 13.00 ± 1.27 g versus vehicle + GDNF 6.84 ± 1.92 g, p = 0.0018, $F_{(1,34)}$ = 8.89, Figure S2D) and PWL (after drug: SCH + GDNF 15.04 ± 1.18 s versus vehicle + GDNF 9.85 ± 0.89 s, p = 0.0353, $F_{(1,32)}$ = 4.99, Figure S2E), but did not impair the animal's locomotor function (Figure S2F). Likewise, knocking down Runx1 in the DRG neuron by intrathecal Runx1 siRNA, as validated by the decreased abundance of Runx1 protein (reduced by ~50% relative to scramble siRNA, p<0.0001, $t_{(6)}$ = 11.21, Figure S2G), significantly prevented the intrathecal GDNF-induced increase in the abundance of P2X3R mRNA (reduced by ~46% relative to

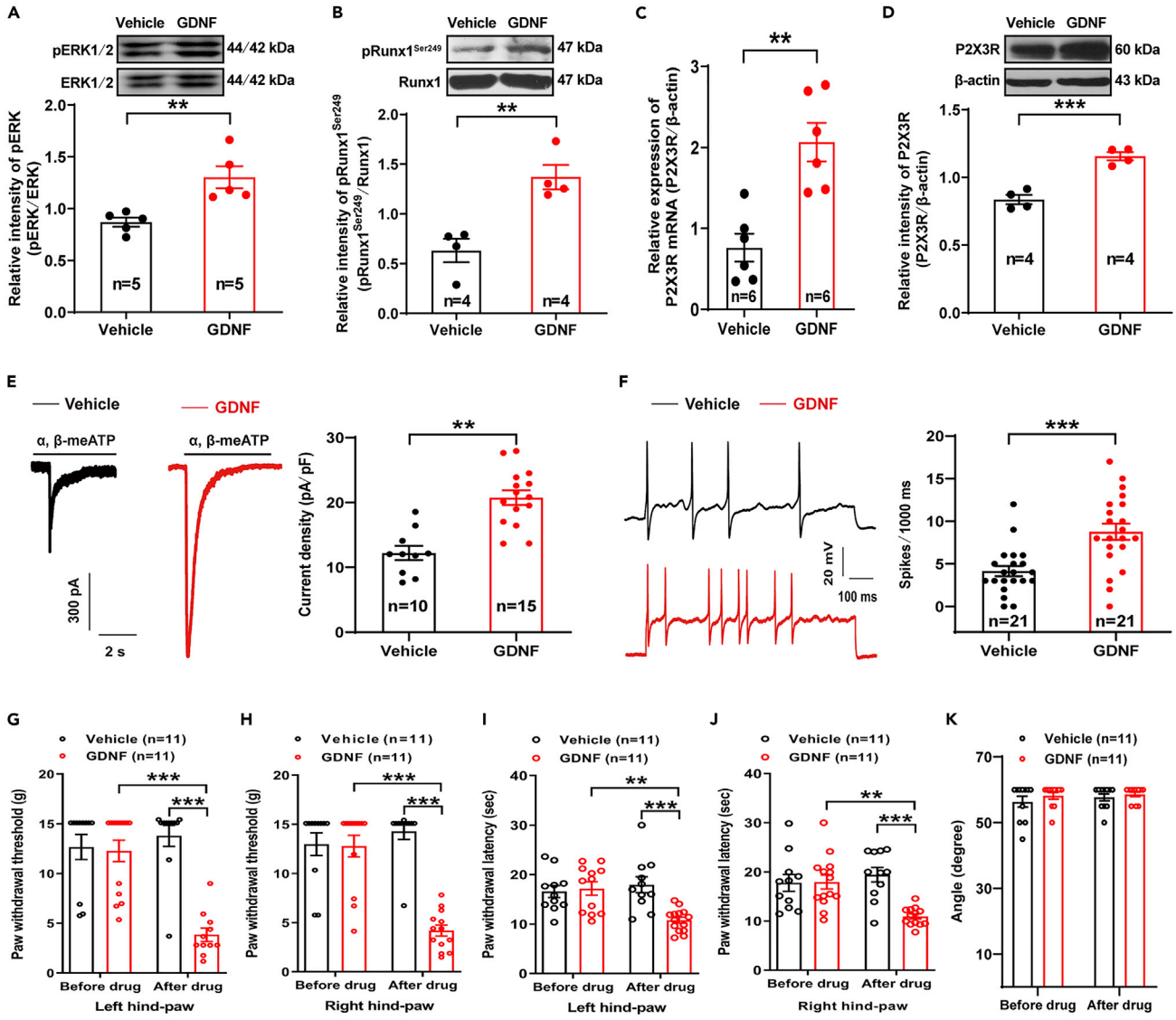

Figure 5. Intrathecal GDNF activates ERK-Runx1 signaling, increases functional P2X3R expression and DRG neurons excitability, and induces pain hypersensitivity in naïve rats

(A) Western blot analysis of phosphorylated ERK abundance in L4/5 DRGs from naïve rats received intrathecal GDNF treatment (200 ng in a 10-μL volume, once per day for three consecutive days) (n = 5 rats per group). Upper: Representative blots are shown.

(B) Western blot of phosphorylated Runx1 abundance in L4/5 DRGs from naïve rats received intrathecal GDNF treatment (n = 4 rats per group). Upper: Representative blots are shown.

(C and D) RT-qPCR and Western blot analyses of P2X3R mRNA (C, n = 6 rats per group) and protein (D, n = 4 rats per group) abundance in L4/5 DRGs from naïve rats with intrathecal GDNF treatment. Upper in (D): Representative blots are shown.

(E and F) Electrophysiological analyses of P2X3R currents (E, n = 10–15 cells from six rats per group) and neuronal excitability (F, n = 21 cells from six rats per group) in L4/5 DRG neurons from naïve rats with intrathecal GDNF treatment. Left in (E) and (F): Representative traces of α,β-meATP-induced P2X3R-currents (E) and neuronal action potentials (F) are shown.

(G–J) Assessment of pain behaviors in naïve rats with intrathecal GDNF treatment at one day after the last drug injection.

(G and H) PWT of left (G) and right (H) hind paw.

(I and J) PWL of left (I) and right (J) hind paw. n = 11 rats per group.

(K) Assessment of animal's locomotor function before and after drug administration (n = 11 rats per group). Data are presented as mean ± SEM. **p<0.01, ***p<0.001, unpaired *t* test for (A)–(F); two-way ANOVA with Sidak's *post hoc* test for (G)–(K). See also Figure S2.

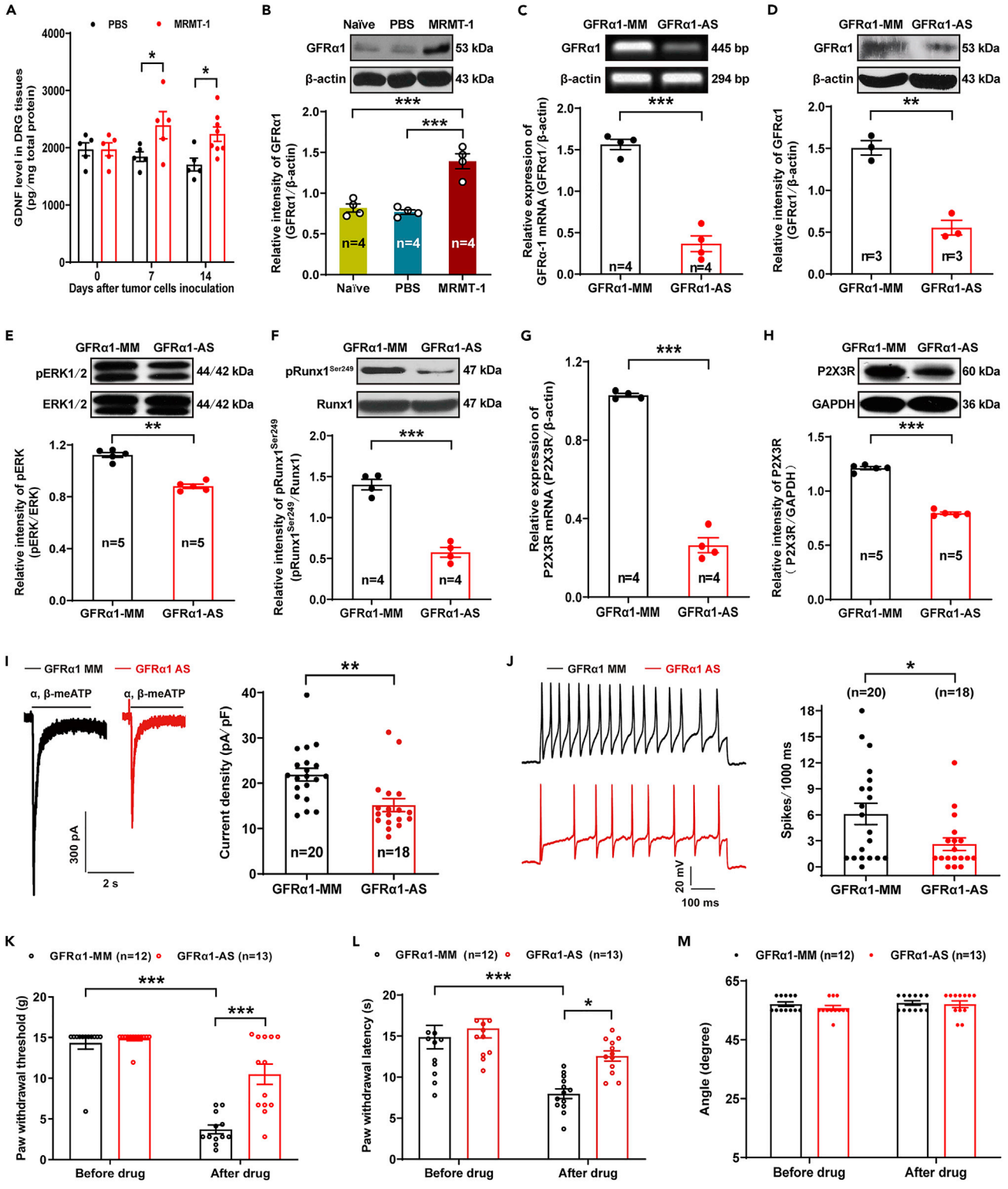

Figure 6. GFRα1 knockdown prevents the activation of ERK-Runx1 signaling, reverses the increase of P2X3R, DRG neurons hyperexcitability, and pain hypersensitivity in bone cancer–bearing rats

(A) Enzyme-linked immunosorbent assay of GDNF content in ipsilateral L4/5 DRGs from PBS- and MRMT-1-treated rats at 14 days after surgery (n = 5–8 rats per group).

Figure 6. *Continued*

(B) Western blot analyses of GFRα1 protein abundance in ipsilateral L4/5 DRGs from naïve, PBS-, and MRMT-1-treated rats at 14 days after surgery (n = 4 rats per group). Upper: Representative blots are shown.

(C and D) RT-qPCR and Western blot analyses of GFRα1 mRNA (C) and protein (D) abundance in ipsilateral L4/5 DRGs from intrathecal GFRα1-MM- and GFRα1-AS-treated rats at 14 days after tumor cells inoculation (n = 3–4 rats per group). Upper: Representative blots are shown.

(E and F) Western blot analyses of phosphorylated ERK (pERK1/2, E) and phosphorylated Runx1 (pRunx1^{Ser249}, F) abundance in ipsilateral L4/5 DRGs from intrathecal GFRα1-MM- and GFRα1-AS-treated rats at 14 days after tumor cells inoculation (n = 4–5 rats per group). Upper: Representative blots are shown.

(G and H) RT-qPCR and Western blot analyses of P2X3R mRNA (G) and protein (H) abundance in ipsilateral L4/5 DRGs from intrathecal GFRα1-MM- and GFRα1-AS-treated rats at 14 days after tumor cells inoculation (n = 4–5 rats per group). Upper in (H): Representative blots are shown.

(I and J) Electrophysiological analyses of P2X3R currents (I) and neuronal excitability (J) in L4/5 DRG neurons from intrathecal GFRα1-MM- and GFRα1-AS-treated rats at 14 days after tumor cells inoculation (n = 18–20 cells from six to seven rats per group). Left in (I) and (J): Representative traces of α,β-meATP-induced P2X3R-currents (I) and neuronal action potentials (J) are shown.

(K and L) Assessment of ipsilateral PWT (K) and PWL (L) from intrathecal GFRα1-MM- and GFRα1-AS-treated rats at 14 days after tumor cells inoculation (n = 12–13 rats per group).

(M) Assessment of animal's locomotor function before and after antisense oligodeoxynucleotide administration (n = 12–13 rats per group). Data are presented as mean ± SEM. *p<0.05, **p<0.01, ***p<0.001, two-way ANOVA with Sidak's *post hoc* test for (A), and (K)–(M); one-way ANOVA with Tukey's *post hoc* test for (B); unpaired *t* test for (C)–(J).

vehicle, p = 0.0105, $t_{(16)}$ = 2.90, Figure S2H) and protein (reduced by ~39% relative to vehicle, p = 0.0025, $t_{(10)}$ = 3.99, Figure S2I) in the DRG neurons and, the pain hypersensitivity as indicated by decreased PWT (on day 8 after drug, siRNA 9.59 ± 1.41 g versus scramble siRNA 2.94 ± 0.74 g, p<0.0001, $F_{(2,72)}$ = 4.77, Figures S2J and S2K) in naïve rats. The inclined-plate test revealed that intrathecal Runx1 siRNA did not impair the animal's locomotor function (Figure S2L). Taken together, these data suggest that exogenous GDNF may be able to promote the P2X3R gene transcription by the activation of ERK-Runx1 signaling cascade, thereby enhancing the neuronal excitability in DRG neurons, and producing pain hypersensitivity in naïve rats.

Knockdown of GFRα1 in DRG neurons prevents the activation of ERK-Runx1 signaling and the upregulation of P2X3R gene transcription, subsequently reduces the neuronal hyperexcitability and pain hypersensitivity in bone metastasis model rats

To validate our hypothesis that activation of GDNF-GFRα1-Ret-ERK signaling is involved in the upregulation of Runx1-mediated P2X3R gene transcription in DRG neurons and in the pathogenesis of pain hypersensitivity in bone cancer rats, we first examined the alterations of GDNF and its membrane receptor GFRα1 in ipsilateral L4/5 DRGs in bone metastasis model rats. Using enzyme-linked immunosorbent assay (ELISA), we found a significant increase of GDNF content (in pg/mg total protein) from day 7 (MRMT-1 2394.48 ± 237.22 versus PBS, 1844.70 ± 85.55, p = 0.0404) to day 14 (MRMT-1 2239.70 ± 125.00 versus PBS 1706.82 ± 112.45, p = 0.0253) after surgery, in ipsilateral L4/5 DRGs of tumor-bearing rats ($F_{(2,27)}$ = 2.33, Figure 6A). Also, the GFRα1 protein abundance was substantially increased (by ~45% versus PBS, p = 0.0002, $F_{(2,9)}$ = 30.39, Figure 6B) in ipsilateral L4/5 DRGs of bone cancer pain rats on day 14 after surgery. Then, we explored the effects of knocking down GFRα1 in DRG neurons, by intrathecal application of GFRα1 antisense oligodeoxynucleotide (GFRα1-AS ODN) as described elsewhere (Dong et al., 2006), on the activation of ERK-Runx1-mediated P2X3R gene transcription, and on the neuronal hyperexcitability and pain hypersensitivity in bone metastasis model rats. Both GFRα1-AS ODN (at a dose of 30 μg dissolved in 10 μL of nuclease-free normal saline) and mismatched ODNs, respectively, were intrathecally administered to bone metastasis model rats on day 7 after tumor cells inoculation, once per day for seven consecutive days, and the following biochemical analysis, electrophysiological recording, and behavioral testing were respectively performed on the day after the last ODN injection. Using RT-qPCR and western blotting analyses, we saw a significant decrease of GFRα1 abundance at both mRNA (reduced by ~77%, p<0.0001, $t_{(6)}$ = 10.57, Figure 6C) and protein (reduced by ~63%, p = 0.0015, $t_{(4)}$ = 7.78, Figure 6D) levels, in ipsilateral L4/5 DRGs of bone cancer rats treated with GFRα1-AS, compared to the mismatched ODN (GFRα1-MM) controls, validating the efficiency of knocking down GFRα1 in DRG neurons by intrathecal GFRα1-AS. Moreover, we observed a significant decrease in the abundance of both pERK (reduced by ~21% relative to GFRα1-MM, p<0.0001, $t_{(8)}$ = 9.63, Figure 6E) and pRunx1^{Ser249} (reduced by ~59% relative to GFRα1-MM, p<0.0001, $t_{(6)}$ = 9.35, Figure 6F) in ipsilateral L4/5 DRGs of bone cancer rats with GFRα1-AS treatment. Consistently, the P2X3R abundance at both mRNA (reduced by ~74%, p<0.0001, $t_{(6)}$ = 19.46, Figure 6G) and protein (reduced by ~34%, p<0.0001, $t_{(8)}$ = 23.08, Figure 6H) levels, the P2X3R current (in pA/pF, GFRα1-AS 15.17 ± 1.44 versus GFRα1-MM 21.89 ± 1.38, p = 0.0018, $t_{(36)}$ = 3.37, Figure 6I), and the neuronal excitability indicated by the AP numbers (in spikes/s, GFRα1-AS 2.61 ± 0.72 versus GFRα1-MM 6.10 ± 1.22,

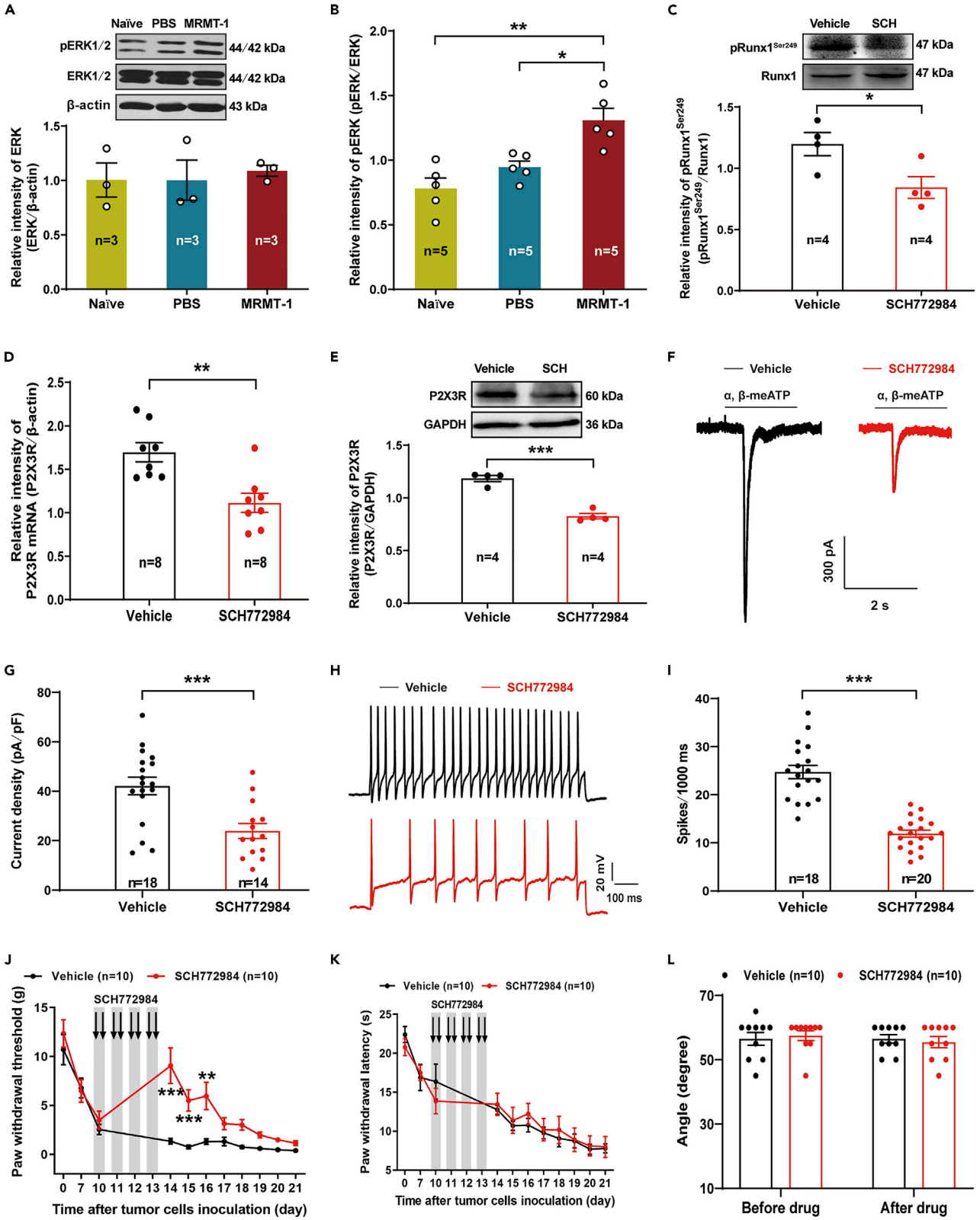
A
Naïve PBS MRMT-1
pERK1/2
ERK1/2
β-actin
44/42 kDa
44/42 kDa
43 kDa
Relative intensity of ERK (ERK/β-actin)
n=3
n=3
n=3
Naïve
PBS
MRMT-1
B
Relative intensity of pERK (pERK/ERK)
n=5
n=5
n=5
C
Vehicle SCH
pRunx1Ser249
Runx1
47 kDa
47 kDa
Relative intensity of pRunx1Ser249 (pRunx1Ser249/Runx1)
n=4
n=4
Vehicle
SCH772984
D
Relative intensity of P2X3R mRNA (P2X3R/β-actin)
n=8
n=8
Vehicle
SCH772984
E
Vehicle SCH
P2X3R
GAPDH
60 kDa
36 kDa
Relative intensity of P2X3R (P2X3R/GAPDH)
n=4
n=4
Vehicle
SCH772984
F
Vehicle
SCH772984
α, β-meATP
α, β-meATP
300 pA
2 s
G
Current density (pA/pF)
n=18
n=14
Vehicle
SCH772984
H
Vehicle
SCH772984
20 mV
100 ms
I
Spikes/1000 ms
n=18
n=20
Vehicle
SCH772984
J
Vehicle (n=10)
SCH772984 (n=10)
SCH772984
Paw withdrawal threshold (g)
Time after tumor cells inoculation (day)
K
Vehicle (n=10)
SCH772984 (n=10)
SCH772984
Paw withdrawal latency (s)
Time after tumor cells inoculation (day)
L
Vehicle (n=10)
SCH772984 (n=10)
Angle (degree)
Before drug
After drug

Figure 7. ERK inhibitor prevents Runx1 activation and functional upregulation of P2X3R, and reverses DRG neurons hyperexcitability and pain hypersensitivity in bone cancer–bearing rats

(A and B) Western blot analyses of ERK (A) and phosphorylated ERK (B) abundance in ipsilateral L4/5 DRGs from naïve, PBS-, and MRMT-1-treated rats at 14 days after surgery (n = 3–5 rats per group). Upper in (A): Representative blots are shown.

(C) Western blot analyses of phosphorylated Runx1 (pRunx1^{Ser249}) abundance in ipsilateral L4/5 DRGs from intrathecal SCH772984- and vehicle-treated rats at 14 days after tumor cells inoculation (n = 4 rats per group). Upper: Representative blots are shown.

(D and E) RT-qPCR and Western blot analyses of P2X3R mRNA (D, n = 8 rats per group) and protein (E, n = 4 rats per group) abundance in ipsilateral L4/5 DRGs from intrathecal SCH772984- and vehicle-treated rats at 14 days after tumor cells inoculation. Upper in (E): Representative blots are shown.

(F–I) Electrophysiological analyses of P2X3R currents (F and G) and neuronal excitability (H and I) in L4/5 DRG neurons from intrathecal SCH772984- and vehicle-treated rats at 14 days after tumor cells inoculation (n = 14–20 cells from six rats per group).

(F) and (H): Representative traces of α,β-meATP-induced P2X3R-currents (F) and neuronal action potentials (H) are shown.

(J and K) Assessment of ipsilateral PWT (J) and PWL (K) from tumor-bearing rats received intrathecal SCH772984 or vehicle treatment (n = 10 rats per group).

(L) Assessment of animal's locomotor function before and after drug administration (n = 10 rats per group). Data are presented as mean ± SEM. *p<0.05, **p<0.01, ***p<0.001, one-way ANOVA with Tukey's *post hoc* test for (A), (B); unpaired *t* test for (C)–(I); repeated-measures two-way ANOVA with Sidak's *post hoc* test for (J) and (K); two-way ANOVA with Sidak's *post hoc* test for (L). See also Figure S3.

p = 0.0223, $t_{(36)}$ = 2.39, Figure 6J), were concomitantly and substantially decreased in ipsilateral L4/5 DRGs of bone cancer rats with GFRα1-AS treatment. Last and likewise, the augmented pain hypersensitivity inferred from decreased PWT (after drug: GFRα1-AS 10.50 ± 1.25 g versus GFRα1-MM 3.72 ± 0.54 g, p<0.0001, $F_{(1,46)}$ = 15.34, Figure 6K) and PWL (after drug: GFRα1-AS 12.57 ± 0.62 s versus GFRα1-MM 7.98 ± 0.60 s, p = 0.0164, $F_{(1,46)}$ = 2.95, Figure 6L) in bone cancer rats was effectively abrogated by intrathecal GFRα1-AS, and the animal's locomotor function was not impaired after the intrathecal GFRα1-AS application (Figure 6M). These results indicate that knocking down GFRα1 prevents the activation of ERK-Runx1 signaling and the upregulation of P2X3R gene transcription in the DRG neurons, subsequently repressing the neuronal hyperexcitability and pain hypersensitivity in bone cancer rats.

Disrupting the activation of ERK-Runx1 signaling in DRG neurons abrogates the enhanced P2X3R gene transcription, and reduces the neuronal hyperexcitability and pain hypersensitivity in bone metastasis model rats

Finally, to determine whether the activation of ERK-Runx1 signaling in DRG neurons is involved in the upregulation of P2X3R gene transcription, as well as in the enhanced neuronal excitability and pain hypersensitivity in bone cancer rats, we examined the effects of either inhibiting ERK activation or disrupting Runx1 phosphorylation, on expression of P2X3R mRNA and protein, and on DRG neurons excitability and pain sensitivity in bone metastasis model rats. The ERK inhibitor SCH772984 (15 μM × 10 μL) was intrathecally administered to tumor-bearing rats on day 10 after tumor cells inoculation, twice per day for four consecutive days, whereas the interfering peptide TAT-Ser or its control peptide TAT-Ala was intrathecally injected to bone metastasis model rats by osmotic pump (25 ng per rat) for seven consecutive days, on day 7 after tumor cells inoculation, and the following biochemical analysis and electrophysiological recording were respectively performed on day 14 after tumor cells inoculation. In fact, using western blotting analysis, we found a substantially increase in the level of phosphorylated ERK (by ~28% versus PBS, p = 0.0148, $F_{(2,12)}$ = 12.50, Figures 7A and 7B) in ipsilateral L4/5 DRGs of MRMT-1 tumor-bearing rats on day 14 after tumor cells inoculation, indicating the activation of ERK signaling in bone cancer rats. Supporting our idea that the activation of ERK signaling is involved in the phosphorylated modification of Runx1, which affects the stabilization and transcriptional activity of Runx1 itself (Chuang et al., 2016; Goyama et al., 2015; Ito et al., 2015; Lie et al., 2020), we indeed found that intrathecal administration of the ERK inhibitor SCH772984 significantly reduced the abundance of pRunx1^{Ser249} (decreased by ~30% relative to vehicle, p = 0.0343, $t_{(6)}$ = 2.73, Figure 7C) in ipsilateral L4/5 DRGs of MRMT-1 rats, indicating that the phosphorylated modification of Runx1 in DRG neurons is dependent upon the activation of ERK signaling in bone cancer rats. Moreover, we found that the increased P2X3R abundance in ipsilateral L4/5 DRGs of MRMT-1 rats were both reversed, at mRNA (decreased by ~34% relative to vehicle, p = 0.0022, $t_{(14)}$ = 3.73, Figure 7D) and protein (decreased by ~30% relative to vehicle, p = 0.0001, $t_{(6)}$ = 8.90, Figure 7E) levels, by intrathecal application of SCH772984. Also, the increased P2X3R current (in pA/pF, SCH 23.95 ± 3.06 versus vehicle 42.12 ± 3.56, p = 0.0008, $t_{(30)}$ = 3.74, Figures 7F and 7G) and the enhanced neuronal excitability (in spikes/sec, SCH 11.90 ± 0.72 versus vehicle 24.72 ± 1.39, p<0.0001, $t_{(36)}$ = 8.42, Figures 7H and 7I) in ipsilateral small-diameter DRG neurons of bone cancer rats, and the augmented pain hypersensitivity in bone metastasis model rats, indicated by decreased PWT (SCH 9.06 ± 1.82 g versus vehicle 1.34 ± 0.29 g, on day 14 after surgery, p<0.0001, $F_{(10,198)}$ = 3.88, Figure 7J) rather than PWL ($F_{(10,198)}$ = 0.42, Figure 7K), were abrogated by intrathecal SCH772984. The inclined-plate test revealed that the animal's locomotor function was not impaired after the intrathecal SCH772984 application (Figure 7L).

Similarly, disruption of Runx1 phosphorylation by using the interfering peptide targeting serine 249 site of Runx1 (TAT-Ser), which was validated by the decreased abundance of pRunx1^{Ser249} (by ~46% relative to TAT-Ala control peptide, p = 0.0005, $t_{(4)}$ = 10.46, Figure S3A) in ipsilateral L4/5 DRGs of bone cancer rats with intrathecal TAT-Ser treatment, effectively restored the bone metastasis-induced upregulation of P2X3R gene transcription, as well as the enhanced neuronal excitability and pain hypersensitivity in tumor-bearing rats (Figures S3B–S3G). The P2X3R abundance was substantially decreased at both mRNA (reduced by ~33% relative to TAT-Ala control peptide, p = 0.0105, $t_{(14)}$ = 2.95, Figure S3B) and protein (reduced by ~32% relative to TAT-Ala control peptide, p = 0.0500, $t_{(4)}$ = 2.78, Figure S3C) levels, in ipsilateral L4/5 DRGs of tumor-bearing rats treated with TAT-Ser peptide. Consistently, the α,β-meATP-induced P2X3R current (in pA/pF, TAT-Ser 27.54 ± 1.72 versus TAT-Ala 37.07 ± 3.33, p = 0.0093, $t_{(25)}$ = 2.82, Figure S3D), and the neuronal excitability (in spikes/sec, TAT-Ser 11.12 ± 1.40 versus TAT-Ala 18.38 ± 1.67, p = 0.0023, $t_{(28)}$ = 3.35, Figure S3E) were both decreased in ipsilateral small-diameter DRG neurons of bone cancer rats treated with TAT-Ser peptide. The behavioral tests revealed that the tumor-induced pain hypersensitivity in bone cancer rats, inferred from a decreased PWT (TAT-Ser 9.97 ± 1.86 g versus TAT-Ala 2.97 ± 0.59 g, p<0.0001 for day 14 after surgery, $F_{(6,119)}$ = 6.35, Figure S3F) rather than PWL (p = 0.5315 for day 14 after surgery, $F_{(6,126)}$ = 1.93, Figure S3G), was significantly abrogated by intrathecal application of TAT-Ser peptide. The inclined-plate test revealed that the animal's locomotor function was not impaired after the intrathecal TAT-Ser peptide application (p = 0.8001, $F_{(1,34)}$ = 0.0008, Figure S3H).

Taken together, these results suggest that disrupting the activation of ERK-Runx1 signaling in DRG neurons abrogates the enhanced P2X3R gene transcription, and reduces the neuronal hyperexcitability and pain hypersensitivity in bone metastasis model rats. Therefore, the upregulation of Runx1-mediated P2X3R gene transcription, induced by the activation of GDNF- GFRα1-Ret-ERK signaling, likely underlies the neuronal hyperexcitability of nociceptive DRG neurons and the pain hypersensitivity in tumor-bearing rats.

DISCUSSION

In this study, we provide multiple lines of evidence to show that the Runx1-mediated P2X3R gene transcription via the activation of GDNF-GFRα1-Ret-ERK signaling contributes to the sensitization of DRG neurons and the development of cancer-associated pain. First, we attested that the transcription factor Runx1 could directly upregulate the transcriptional activity of P2X3R gene promoter in PC12 cells, and the upregulation of Runx1-mediated P2X3R gene transcription attributes the sensitization of DRG neurons and the cancer pain development. Serving as a Runt domain transcription factor, Runx1 is implicated in controlling the differentiation of nociceptors that express the neurotrophin receptor Ret, and regulating the expression of many ion channels and receptors in DRG neurons, including ATP-gated P2X3R (Chen et al., 2006; Ugarte et al., 2012). In line with this understanding, we indeed found a colocalization of P2X3R with Runx1 in the DRG neurons, and an enhanced expression of both P2X3R and Runx1 in cancer-bearing rat DRG neurons, raising the possibility that Runx1 may serve as a regulator for P2X3R gene transcription. Actually, our results from transient transfection experiments in PC12 cells further support this conception to show that Runx1 directly promotes the P2X3R gene promoter activity in these cells. Moreover, because the phosphorylated modification of Runx1 by activating MAPK/ERK signaling (Bae and Lee, 2006; Hamelin et al., 2006; Ito, 1999; Kanno et al., 1998) is known to affect the stabilization and transcriptional activity of Runx1 itself (Chuang et al., 2016; Goyama et al., 2015; Ito et al., 2015; Lie et al., 2020), the elevated level of phosphorylated Runx1 at serine 249 residue (pRunx1^{Ser249}) in ipsilateral L4/5 DRGs convincingly implies an enhanced transcriptional activity of Runx1 in bone metastasis model rats, which may underlie the upregulation of Runx1-mediated P2X3R gene transcription at these conditions. In fact, it has been shown that the P2X3R gene promoter activity is upregulated by the transcription factor Runx1 that specifically interacts with the P2X3R proximal gene promoter region (Ugarte et al., 2012), and that an enrichment of Runx1 at the P2X3R gene promoter accompanying increased P2X3R gene transcription is seen in a rat model of the complete Freund's adjuvant (CFA)-induced inflammatory pain (Nunez-Badinez et al., 2018). In addition, Runx1 is implicated to regulate several pain responses, including inflammatory pain and neuropathic pain (Abdel Samad et al., 2010; Chen et al., 2006; Kobayashi et al., 2012; Kramer et al., 2006; Marmigère et al., 2006; Yoshikawa et al., 2007). Mice lacking Runx1 exhibit specific defects in thermal and neuropathic pain (Chen et al., 2006), whereas postnatal activation of Runx1 increases the sensitivity to neuropathic pain (Kanaykina et al., 2010). We here demonstrated that knocking down Runx1 in DRG neurons suppresses P2X3R gene transcription, and attenuates the neuronal hyperexcitability and pain hypersensitivity in tumor-bearing rats, whereas overexpressing Runx1 in DRG neurons promotes P2X3R gene transcription, and enhances the neuronal excitability and pain sensitivity in naïve rats. We acknowledge that lentiviral

transduction is not neuron-specific, and satellite glial cells in the DRGs may also be transduced in the experiments of Runx1 overexpression. However, because both Runx1 (Chen et al., 2006; Kobayashi et al., 2012; Kramer et al., 2006; Yoshikawa et al., 2007) and P2X3R (Bradbury et al., 1998; Chen et al., 1995, 2008, 2012) are mainly expressed in DRG neurons but not in satellite glial cells, thus the effects of lentivirus-mediated Runx1 overexpression on the upregulation of P2X3R expression and activity mainly result from the activation of DRG neurons rather than the satellite glial cells in the DRGs. Collectively, all these findings provide direct evidence to support our hypothesis that the Runx1-mediated P2X3R gene transcription contributes to the increased expression of P2X3R in DRG neurons, and underlies the neuronal hyperexcitability and pain hypersensitivity in bone metastasis model rats.

Of course, changes in input resistance (e.g., through Runx1-mediated regulation of the expression of potassium channels) could directly cause a decrease or an increase in the current amplitude of ion channels on the neuronal membrane, without any impact on the expression of the channels. However, the P2X3R is a ligand-gated ion channel which is activated specifically by its natural ligand, the extracellular ATP *in vivo* (Surprenant and North, 2009). Most of the P2X3R agonists are derived from the modification of the ATP molecule, e.g., α,β-meATP. When recording P2X3R currents, the cell was held at −60 mV, which is closed to the resting membrane potential of the cell. A specific agonist, α,β-meATP, was applied to evoke the P2X3R currents in a single-cell scale, and the P2X3R current is validated by its fast inactivation characteristics (Petruska et al., 2000; Wirkner et al., 2007) as shown in the Figures 2D and 3G in our present study. In addition, we indeed found an increased expression of P2X3R in the ipsilateral L4/5 DRG neurons of tumor-bearing rats at 14 days after surgery, whereas knock-down and overexpression of Runx1 could decrease and increase P2X3R expression respectively, and correspondingly reduce and enhance the P2X3R currents. Therefore, we suggest that the Runx1-mediated P2X3R gene transcription may explain the increase of P2X3R expression and P2X3R currents.

In the present study, the L4/5 DRGs were examined based on the previous findings showed that sciatic DRG neurons were normally located in lumbar ganglia L3-L6, and nearly 98–99% of all sciatic DRG perikaryal resided in the L4 and L5 DRGs (Swett et al., 1991), where L4 DRG contains somas of the majority of neurons with receptive fields in the hind paw (da Silva Serra et al., 2016). However, the sensory neurons innervating the periosteum of the tibia are confined predominantly to L3 and L4 DRGs (Gajda et al., 2004), and the soma of sensory neurons innervating the rat tibia are located predominantly in the L3 DRG (Ivanusic, 2009). We acknowledge the limitation of our study that it was not investigated in which afferents (bone, muscle, cutaneous, etc.) the expression of Runx1 and P2X3R is enhanced. Given that the cutaneous afferents innervating the hind paw rather than bone afferents themselves are sensitized in animals with bone cancer pain (de Clauser et al., 2020; Kucharczyk et al., 2020), and the anti-P2X3 antibody only reverses cutaneous, but not skeletal pain hypersensitivity to these animals (Guedon et al., 2016), it raises the possibility that bone afferents are probably not involved in the P2X3R-mediated mechanical hypersensitivity under bone cancer condition. It is suggested that cutaneous afferents at distant sites from the tumor-bearing bone might contribute to secondary mechanical hypersensitivity (de Clauser et al., 2020; Kucharczyk et al., 2020). Further study is needed to determine the involved heterogeneous population of sensory neurons that contribute to nociceptive processing of bone cancer pain.

Also, only small-diameter lumbar DRG neurons were examined in the electrophysiological studies. In spite that P2X3Rs are found mostly expressed in small- and medium-diameter sensory neurons that bind the lectin IB4 (Bradbury et al., 1998), co-expression of P2X3R with $CGRP^+$, or even large-diameter, $NF\text{-}200^+$ DRG neurons has been reported in both animals and human beings (Ruan et al., 2005; Sato et al., 2018; Shiers et al., 2021), especially suffered from chronic nerve injury or with GDNF or NGF treatment (Chao et al., 2008; Ramer et al., 2001). Increased expression of P2X3R on $CGRP^+$ epidermal nerve fibers also was found in mice with bone cancer pain (Gilchrist et al., 2005). It is reported that appropriately 45% of rat DRG neurons show a substantial overlap between $CGRP^+$ peptidergic neurons and $IB4^+$ non-peptidergic nociceptor neurons (Price and Flores, 2007). Although P2X3R are mainly co-localized with $IB4^+$ DRG neurons, there is still almost 20% P2X3R co-expressed with $CGRP^+$ peptidergic DRG neurons in rats (Hu et al., 2020), and the expression of P2X3R in $CGRP^+$ DRG neurons is significantly increased in rats with diabetic neuropathic pain (He et al., 2020a). On the other side, TRPV1 is highly co-expressed with CGRP in small-sized, peptidergic DRG neurons, whereas occasional $TRPV1^+$, small-sized, non-peptidergic DRG neurons are also expressed IB4 (Salio et al., 2021). TRPV1-immunoreactivity is also found co-localized with staining for the P2X3R, and with binding sites for the lectin IB4 in the DRG neurons of rats (Guo et al., 1999; Shin et al., 2008; Yu et al., 2021). In the

rat lumbar DRG, the *in situ* hybridization histochemistry revealed that most P2X3-positive neurons had Ret mRNA, and about half of them co-expressed TrkA and TRPV1 mRNAs (Kobayashi et al., 2005). These findings suggest that there are, perhaps, small group of $TRPV1^+$ neurons and $CGRP^+$ neurons expressing P2X3Rs in rat DRGs. Thus, we did not differentiate the $IB4^+$ and $CGRP^+$ DRG neurons in our electrophysiological studies because of the wide distribution of P2X3R in non-peptidergic and peptidergic DRG neurons. In fact, the ectopic sprouting of sensory (including $CGRP^+$ and $NF200^+$) and sympathetic nerve fibers by NGF (Bloom et al., 2011; Jimenez-Andrade et al., 2010; Lindsay et al., 2005; Mantyh, 2019; Mantyh et al., 2010), as well as a role of osteoclasts known to express a range of P2X receptors may also be important for the development of bone cancer pain [see (Jørgensen, 2019; Rumney et al., 2012) for review]. In addition, we cannot assure that all the recorded small-diameter DRG neurons in our experiments are nociceptive sensory neurons. In our previous study (Zheng et al., 2012), together with immunostaining and single-cell reverse-transcriptase PCR analysis, we have demonstrated that in acute isolated small-diameter DRG neurons, the majority were $IB4^+$ and $CGRP^+$ neurons, most of them also expressed the nociceptive marker, TRPV1. Moreover, we found that in all recorded small-diameter DRG neurons, the major proportion also were $TRPV1^+$ neurons and $CGRP^+$ neurons, suggesting that most recorded small-diameter DRG neurons in our experiments are nociceptive neurons. Certainly, validation of nociceptive sensory neurons using capsaicin is needed for all electrophysiological recorded DRG neurons in the future study.

Moreover, application of 20 μM α,β-meATP is not selective for P2X3 ATP receptors. It is noteworthy that α,β-meATP is an agonist at P2X1, P2X3 and P2X2/3 receptors, but at not other type of P2X receptor-channels (Chizh and Illes, 2001). In rat cultured DRG neurons, the electrophysiological data revealed that the α,β-meATP (100 nM–100 μM) evokes transient inward currents, and the EC_{50} is 1.95 μM (Robertson et al., 1996). The concentration of α,β-meATP producing half-maximal activation (EC_{50}) of neurons with fast desensitization (i.e. P2X3R) is less (11 μM) than that of neurons with slow desensitization (i.e. P2X2/3 receptors) (63 μM) (Ueno et al., 1999). Therefore, α,β-meATP at 10–30 μM is usually applied for evoking the maximum P2X3R currents but not P2X2/3 receptors currents in most electrophysiological experiments (Burgard et al., 1999; Qiao et al., 2022; Ueno et al., 1999; Xiang et al., 2008). In addition, the upregulation of other P2X receptor subtypes in this pain model was not investigated, and the 20 μM α,β-meATP may also act these P2X receptor subtypes besides P2X3R.

Second, we identified that the activation of GFRα-Ret-ERK signaling by GDNF is involved in Runx1-mediated P2X3R gene transcription and cancer pain development in bone metastasis model rats. In SH-SY5Y human neuroblastoma cells expressing endogenous GFRα1 and Ret (Fukuda et al., 2002), we provide direct evidence to show that GDNF promotes the Runx1-mediated P2X3R gene transcription via the activation of ERK signaling. It is known that Runx1 is expressed in most nociceptors during embryonic development but in adult mice, becomes restricted to nociceptors marked by expression of the neurotrophin receptor Ret (Chen et al., 2006). As a receptor tyrosine kinase, Ret is activated by GDNF binding to GFRα1, which in turn activates various intracellular signaling pathways, including RAS/ERK signaling (Hayashi et al., 2000; Kawai and Takahashi, 2020; Plaza-Menacho et al., 2006). We thus speculate that the activation of ERK signaling, which is known important for the phosphorylated modification of Runx1 and its transcriptional activity (Chuang et al., 2016; Goyama et al., 2015; Ito et al., 2015; Lie et al., 2020), is likely involved in Runx1-mediated P2X3R gene transcription by GDNF in bone metastasis model rats. Supporting our speculation, we indeed found that in cultured DRG neurons, exogenous GDNF prominently activates the ERK-Runx1 signaling and subsequently elevates the levels of P2X3R mRNA and protein, and more importantly, all these actions of GDNF are blocked respectively by the GDNF antibody, the Ret inhibitor, and the ERK inhibitor, but not by the Src-family tyrosine kinases inhibitor or the PI3K inhibitor. Similarly, in the *in vivo* experiments we also found that intrathecal GDNF activates the ERK-Runx1 signaling, subsequently promotes P2X3R gene transcription and protein expression and, increases P2X3R current and neuronal excitability in DRG neurons, and induces pain hypersensitivity in naïve rats. We suggest that the activation of ERK-Runx1 signaling is required for intrathecal GDNF-mediated P2X3R gene transcription and pain hypersensitivity based on the evidence that pretreatment with ERK inhibitor or Runx1 siRNA prevents all effects of intrathecal GDNF on P2X3R mRNA and protein expression and pain sensitivity in naïve rats.

It has been reported that GDNF can sensitize nociceptors and induce behavioral hyperalgesia in an inflammatory pain model (Malin et al., 2006), and an increased expression of GDNF was found in the spinal cord of some pain models (Fang et al., 2003). However, opposing results have been found regarding GDNF in bone cancer pain (Ding et al., 2017; Meng et al., 2015). In a rat model of bone cancer pain induced by tibia

injection of Walker 256 rat mammary gland carcinoma cells, Ding et al. (2017) reported that GDNF expression was selectively reduced in the ipsilateral L3 DRG and lumbar spinal cord on day 16 after tumor cells inoculation, and restoration of GDNF expression in the spinal cord alleviated hyperalgesia. Whereas in a rat model of bone cancer pain induced by intratibial MRMT-1 inoculation, Meng et al. (2015) showed that the downregulation of GDNF expression by intrathecal injection of lentivirus-mediated GDNF RNAi relieves bone cancer-induced hyperalgesia in rats. In the current study, we found a significant increase of GDNF content in the ipsilateral L4/5 DRGs and the involvement of activated GDNF signaling in bone cancer pain. Discrepancies between the work of Ding et al. and the findings of Meng et al. and our study may be due to differences in the tumor cells/DRG location (segmental levels)/measuring methods/observed time, and/or differences in environmental or husbandry conditions in the animal facilities.

Inflammatory bone pain, which usually emerges in bone cancer, involves activation and sensitization of non-peptidergic bone afferent neurons via GDNF-GFRα1 signaling pathway (Nencini et al., 2018). An increased expression of GFRα1 at mRNA and protein levels was observed in DRG neurons after peripheral nerve injury (Bennett et al., 2000; Kashiba et al., 1998; Keast et al., 2010). Our findings of the elevated content of GDNF, the increased abundance of GFRα1 and, the phosphorylated ERK and Runx1, in ipsilateral L4/5 DRGs of tumor-bearing rats, strongly supported the activation of GDNF-GFRα1-ERK-Runx1 signaling in the DRG neurons of bone cancer pain rats. In agreement with these findings, we found that knocking down GFRα1 in DRG neurons by intrathecal GFRα1-AS ODN (Dong et al., 2006) indeed prevents the activation of ERK-Runx1 signaling and the upregulation of P2X3R gene transcription in DRG neurons, subsequently repressing the neuronal hyperexcitability and pain hypersensitivity in bone metastasis model rats. Likewise, disrupting the activation of ERK-Runx1 signaling in DRG neurons, either by intrathecal ERK inhibitor or by intrathecal interfering peptide targeting serine 249 site of Runx1 (TAT-Ser), abrogates the enhanced P2X3R gene transcription, and reduces the neuronal hyperexcitability and pain hypersensitivity in bone cancer pain model rats. Taken together, these data provide solid evidence demonstrating that the activation of GDNF-GFRα1-Ret-ERK signaling is involved in the upregulation of Runx1-mediated P2X3R gene transcription in DRG neurons and in the pathogenesis of pain hypersensitivity in bone cancer rats.

Of note, the source of increased GDNF concentration detected in DRG tissues was not examined. DRG sensory neurons are suggested as one of the origins of accumulated GDNF in the transected sciatic nerve, where a subgroup of small- to medium-sized DRG neurons synthesized GDNF-containing dense-cored vesicles in the neuronal somata and anterogradely transports the vesicles to the nerve terminals (Ohta et al., 2001). Moreover, GDNF mRNA and protein expression are increased in Schwann cells and DRG satellite cells after chronic sciatic nerve injury (Chao et al., 2008; Hammarberg et al., 1996), and these glia-derived GDNF is taken up by DRG neurons, and transported anterogradely along the axons for release from terminals (Rind and von Bartheld, 2002). Additionally, GDNF can be secreted by pre-osteoclasts to mediate osteoclast-osteoblast crosstalk by regulating bone marrow mesenchymal stem cells (BMSC) migration and osteogenesis (Yi et al., 2020). BMSC can also inhibit neuroinflammation by secreting GDNF to regulate microglial polarization, thereby alleviating deafferentation pain in rats (Zhong et al., 2020). Neuroinflammation, which may occur during bone cancer pain, has been reported to induce GDNF expression in activated astrocytes, microglia, and infiltrating macrophages [see (Duarte Azevedo et al., 2020) for review]. Some reports also describe the upregulation of Ret and GFRα1 in glial cells under pathological conditions [see (Duarte Azevedo et al., 2020) for review], suggesting that potential non-neuronal mechanism as play as well.

Besides, we cannot give a clear explanation regarding why the relief from thermal hyperalgesia is not evident after interfering the ERK-Runx1 signaling, in spite that intrathecal exogenous GDNF produced mechanical hypersensitivity and thermal hyperalgesia in naïve rats, and GFRα1-AS abrogated the augmented pain hypersensitivity including both mechanical hypersensitivity and thermal hyperalgesia in bone cancer rats. The discrepancy observed between the reversal of thermal hyperalgesia with GDNF/GFRα1-AS might be explained by the activation of downstream pathways other than ERK signaling. In the present study, it was only shown that ERK mediates P2X3R upregulation by GDNF, but the contributions of other signaling cascades to bone cancer pain can't be excluded. Moreover, in Runx1 knockout mice the thermal thresholds are increased (Chen et al., 2006), and that blockade of P2X3R reduces thermal and mechanical hyperalgesia in several models of acute and chronic pain (He et al., 2020b; Liu et al., 2013; McGaraughty et al., 2003). Hence, other transcriptional targets than P2X3R might contribute to the fact that thermal hyperalgesia was not affected by interfering the ERK-Runx1 signaling. The potential mechanisms underlying thermal hyperalgesia for bone cancer pain are needed to investigate in the future study.

In conclusion, this study demonstrates that the Runx1-mediated P2X3R transcription via the activation of GDNF-GFRα-Ret-ERK signaling contributes to the sensitization of DRG neurons and the pathogenesis of bone cancer pain. Our findings identify a potentially targetable mechanism that may cause bone metastasis-associated pain in cancer patients.

Limitations of the study

There are some limitations to this study. First, the present study was conducted using female animals alone with a single rat mammary gland tumor cell line model of bone metastasis, thus the generalizability to bone metastases that would be commonly encountered with males is limited. Also, the tumor cell-nerve interactions are variable depending on the tumor cell type. Therefore, other models of tumor cells bone metastasis that are suitable for male animals, such as the Dunning (R-3327) rat prostate adenocarcinoma model (Liepe et al., 2005) or the fibrosarcoma cells (NCTC 2472) mouse model (Wacnik et al., 2001), are needed to explore in the future study.

Second, for RT-qPCR experiments, levels of actin mRNA are not very stable in the DRG of neuropathy models (Bangaru et al., 2012) and might also be affected in the cancer model, particularly considering that the nerve fibers undergo cycles of sprouting, degeneration and re-sprouting which might affect cytoskeletal transcript/protein levels (Mantyh, 2013). Therefore, at least 2 housekeeping genes (HKGs) [e.g., MAPK6 and GAPDH, which have been identified as the two most stable HKGs for normalizing gene expression for RT-qPCR analysis in the context of peripheral nerve injury (Bangaru et al., 2012)] need to be used in the future study to obtain accurate expression levels of the target genes (Vandesompele et al., 2002), and a prior analysis of HKG expression levels is important for accurate normalization of gene expression in models of nerve injury (Bangaru et al., 2012).

STAR★METHODS

Detailed methods are provided in the online version of this paper and include the following:

- KEY RESOURCES TABLE
- RESOURCE AVAILABILITY
  - Lead contact
  - Materials availability
  - Data and code availability
- EXPERIMENTAL MODEL AND SUBJECT DETAILS
  - Animals
- METHOD DETAILS
  - Plasmid construction, transient transfections and reporter assays
  - Animal model of bone cancer pain
  - Intrathecal catheterization
  - Drug administration and lentivirus infection
  - Behavioral tests
  - Primary culture and acute dissociation of DRG neurons
  - RNA extraction and RT-qPCR
  - Western blotting
  - Enzyme-linked immunosorbent assay
  - Immunofluorescence staining
  - Electrophysiology
- QUANTIFICATION AND STATISTICAL ANALYSIS

SUPPLEMENTAL INFORMATION

Supplemental information can be found online at https://doi.org/10.1016/j.isci.2022.104936.

ACKNOWLEDGMENTS

This work was supported by the grants from National Key R&D Program of China (2019YFC1712104) and National Natural Science Foundation of China (82171226, 81974169, 81671085), Natural Science Foundation of Beijing Municipality (7222105), China, and King's College London (KCL)–Peking University Health Science Center (PKUHSC) Joint Institute for Medical Research (JI) program (BMU2021KCL001), China.

We thank Dr. Martin Montecino (University of Andres Bello, Santiago, Chile) for providing the p1934-p2x3-luc, p415-p2x3-luc, and pCDNA3.1-Runx1 plasmids.

AUTHOR CONTRIBUTIONS

G.G.X. designed research. Z.L.Y., X.D.L., and Z.X.Z. performed experiments. S.L., Y.T., K.X., J.C., X.M.Y., and M.L. analyzed data. G.G.X. and Z.L.Y. drafted the manuscript. All authors commented on and approved the final draft.

DECLARATION OF INTERESTS

The authors declare no competing interests.

Received: April 22, 2022
Revised: July 15, 2022
Accepted: August 10, 2022
Published: September 16, 2022

REFERENCES

Abdel Samad, O., Liu, Y., Yang, F.C., Kramer, I., Arber, S., and Ma, Q. (2010). Characterization of two Runx1-dependent nociceptor differentiation programs necessary for inflammatory versus neuropathic pain. Mol. Pain *6*, 45. https://doi.org/10.1186/1744-8069-6-45.

Alvarez, P., Chen, X., Bogen, O., Green, P.G., and Levine, J.D. (2012). IB4(+) nociceptors mediate persistent muscle pain induced by GDNF. J. Neurophysiol. *108*, 2545–2553. https://doi.org/10.1152/jn.00576.2012.

Andriessen, A.S., Donnelly, C.R., and Ji, R.R. (2021). Reciprocal interactions between osteoclasts and nociceptive sensory neurons in bone cancer pain. Pain Rep. *6*, e867. https://doi.org/10.1097/pr9.0000000000000867.

Bae, S.C., and Lee, Y.H. (2006). Phosphorylation, acetylation and ubiquitination: the molecular basis of RUNX regulation. Gene *366*, 58–66. https://doi.org/10.1016/j.gene.2005.10.017.

Bangaru, M.L.Y., Park, F., Hudmon, A., McCallum, J.B., and Hogan, Q.H. (2012). Quantification of gene expression after painful nerve injury: validation of optimal reference genes. J. Mol. Neurosci. *46*, 497–504. https://doi.org/10.1007/s12031-011-9628-x.

Bennett, D.L., Boucher, T.J., Armanini, M.P., Poulsen, K.T., Michael, G.J., Priestley, J.V., Phillips, H.S., McMahon, S.B., and Shelton, D.L. (2000). The glial cell line-derived neurotrophic factor family receptor components are differentially regulated within sensory neurons after nerve injury. J. Neurosci. *20*, 427–437. https://doi.org/10.1523/jneurosci.20-01-00427.2000.

Bernier, L.P., Ase, A.R., and Séguéla, P. (2018). P2X receptor channels in chronic pain pathways. Br. J. Pharmacol. *175*, 2219–2230. https://doi.org/10.1111/bph.13957.

Bloom, A.P., Jimenez-Andrade, J.M., Taylor, R.N., Castañeda-Corral, G., Kaczmarska, M.J., Freeman, K.T., Coughlin, K.A., Ghilardi, J.R., Kuskowski, M.A., and Mantyh, P.W. (2011). Breast cancer-induced bone remodeling, skeletal pain, and sprouting of sensory nerve fibers. J. Pain *12*, 698–711. https://doi.org/10.1016/j.jpain.2010.12.016.

Bradbury, E.J., Burnstock, G., and McMahon, S.B. (1998). The expression of P2X3 purinoreceptors in sensory neurons: effects of axotomy and glial-derived neurotrophic factor. Mol. Cell. Neurosci. *12*, 256–268. https://doi.org/10.1006/mcne.1998.0719.

Burgard, E.C., Niforatos, W., van Biesen, T., Lynch, K.J., Touma, E., Metzger, R.E., Kowaluk, E.A., and Jarvis, M.F. (1999). P2X receptor-mediated ionic currents in dorsal root ganglion neurons. J. Neurophysiol. *82*, 1590–1598. https://doi.org/10.1152/jn.1999.82.3.1590.

Chao, T., Pham, K., Steward, O., and Gupta, R. (2008). Chronic nerve compression injury induces a phenotypic switch of neurons within the dorsal root ganglia. J. Comp. Neurol. *506*, 180–193. https://doi.org/10.1002/cne.21537.

Chaplan, S.R., Bach, F.W., Pogrel, J.W., Chung, J.M., and Yaksh, T.L. (1994). Quantitative assessment of tactile allodynia in the rat paw. J. Neurosci. Methods *53*, 55–63. https://doi.org/10.1016/0165-0270(94)90144-9.

Chen, C.C., Akopian, A.N., Sivilotti, L., Colquhoun, D., Burnstock, G., and Wood, J.N. (1995). A P2X purinoceptor expressed by a subset of sensory neurons. Nature *377*, 428–431. https://doi.org/10.1038/377428a0.

Chen, C.L., Broom, D.C., Liu, Y., de Nooij, J.C., Li, Z., Cen, C., Samad, O.A., Jessell, T.M., Woolf, C.J., and Ma, Q. (2006). Runx1 determines nociceptive sensory neuron phenotype and is required for thermal and neuropathic pain. Neuron *49*, 365–377. https://doi.org/10.1016/j.neuron.2005.10.036.

Chen, Y., Li, G., and Huang, L.Y.M. (2012). P2X7 receptors in satellite glial cells mediate high functional expression of P2X3 receptors in immature dorsal root ganglion neurons. Mol. Pain *8*, 9. https://doi.org/10.1186/1744-8069-8-9.

Chen, Y., Zhang, X., Wang, C., Li, G., Gu, Y., and Huang, L.Y.M. (2008). Activation of P2X7 receptors in glial satellite cells reduces pain through downregulation of P2X3 receptors in nociceptive neurons. Proc. Natl. Acad. Sci. USA *105*, 16773–16778. https://doi.org/10.1073/pnas.0801793105.

Chizh, B.A., and Illes, P. (2001). P2X receptors and nociception. Pharmacol. Rev. *53*, 553–568.

Chuang, L.S.H., Khor, J.M., Lai, S.K., Garg, S., Krishnan, V., Koh, C.G., Lee, S.H., and Ito, Y. (2016). Aurora kinase-induced phosphorylation excludes transcription factor RUNX from the chromatin to facilitate proper mitotic progression. Proc. Natl. Acad. Sci. USA *113*, 6490–6495. https://doi.org/10.1073/pnas.1523157113.

Costantini, F. (2010). GDNF/Ret signaling and renal branching morphogenesis: from mesenchymal signals to epithelial cell behaviors. Organogenesis *6*, 252–262. https://doi.org/10.4161/org.6.4.12680.

da Silva Serra, I., Husson, Z., Bartlett, J.D., and Smith, E.S.J. (2016). Characterization of cutaneous and articular sensory neurons. Mol. Pain *12*. 1744806916636387. https://doi.org/10.1177/1744806916636387.

de Clauser, L., Luiz, A.P., Santana-Varela, S., Wood, J.N., and Sikandar, S. (2020). Sensitization of cutaneous primary afferents in bone cancer revealed by in vivo calcium imaging. Cancers *12*, E3491. https://doi.org/10.3390/cancers12123491.

Ding, Z., Xu, W., Zhang, J., Zou, W., Guo, Q., Huang, C., Liu, C., Zhong, T., Zhang, J.M., and Song, Z. (2017). Normalizing GDNF expression in the spinal cord alleviates cutaneous hyperalgesia but not ongoing pain in a rat model of bone cancer pain. Int. J. Cancer *140*, 411–422. https://doi.org/10.1002/ijc.30438.

Dong, Z.Q., Wang, Y.Q., Ma, F., Xie, H., and Wu, G.C. (2006). Down-regulation of GFRalpha-1 expression by antisense oligodeoxynucleotide aggravates thermal hyperalgesia in a rat model of neuropathic pain. Neuropharmacology *50*, 393–403. https://doi.org/10.1016/j.neuropharm.2005.09.015.

Duarte Azevedo, M., Sander, S., and Tenenbaum, L. (2020). GDNF, A neuron-derived factor

upregulated in glial cells during disease. J. Clin. Med. *9*, E456. https://doi.org/10.3390/jcm9020456.

Epner, D.E., Partin, A.W., Schalken, J.A., Isaacs, J.T., and Coffey, D.S. (1993). Association of glyceraldehyde-3-phosphate dehydrogenase expression with cell motility and metastatic potential of rat prostatic adenocarcinoma. Cancer Res. *53*, 1995–1997.

Fang, D., Kong, L.Y., Cai, J., Li, S., Liu, X.D., Han, J.S., and Xing, G.G. (2015). Interleukin-6-mediated functional upregulation of TRPV1 receptors in dorsal root ganglion neurons through the activation of JAK/PI3K signaling pathway: roles in the development of bone cancer pain in a rat model. Pain *156*, 1124–1144. https://doi.org/10.1097/j.pain.0000000000000158.

Fang, M., Wang, Y., He, Q.H., Sun, Y.X., Deng, L.B., Wang, X.M., and Han, J.S. (2003). Glial cell line-derived neurotrophic factor contributes to delayed inflammatory hyperalgesia in adjuvant rat pain model. Neuroscience *117*, 503–512. https://doi.org/10.1016/s0306-4522(02)00958-2.

Franck, M.C.M., Stenqvist, A., Li, L., Hao, J., Usoskin, D., Xu, X., Wiesenfeld-Hallin, Z., and Ernfors, P. (2011). Essential role of Ret for defining non-peptidergic nociceptor phenotypes and functions in the adult mouse. Eur. J. Neurosci. *33*, 1385–1400. https://doi.org/10.1111/j.1460-9568.2011.07634.x.

Fukuda, T., Kiuchi, K., and Takahashi, M. (2002). Novel mechanism of regulation of Rac activity and lamellipodia formation by RET tyrosine kinase. J. Biol. Chem. *277*, 19114–19121. https://doi.org/10.1074/jbc.M200643200.

Gajda, M., Litwin, J.A., Adriaensen, D., Timmermans, J.P., and Cichocki, T. (2004). Segmental distribution and morphometric features of primary sensory neurons projecting to the tibial periosteum in the rat. Folia Histochem. Cytobiol. *42*, 95–99.

Gattenloehner, S., Chuvpilo, S., Langebrake, C., Reinhardt, D., Müller-Hermelink, H.K., Serfling, E., Vincent, A., and Marx, A. (2007). Novel RUNX1 isoforms determine the fate of acute myeloid leukemia cells by controlling CD56 expression. Blood *110*, 2027–2033. https://doi.org/10.1182/blood-2007-02-074203.

Gilchrist, L.S., Cain, D.M., Harding-Rose, C., Kov, A.N., Wendelschafer-Crabb, G., Kennedy, W.R., and Simone, D.A. (2005). Re-organization of P2X3 receptor localization on epidermal nerve fibers in a murine model of cancer pain. Brain Res. *1044*, 197–205. https://doi.org/10.1016/j.brainres.2005.02.081.

Goyama, S., Huang, G., Kurokawa, M., and Mulloy, J.C. (2015). Posttranslational modifications of RUNX1 as potential anticancer targets. Oncogene *34*, 3483–3492. https://doi.org/10.1038/onc.2014.305.

Guedon, J.M.G., Longo, G., Majuta, L.A., Thomspon, M.L., Fealk, M.N., and Mantyh, P.W. (2016). Dissociation between the relief of skeletal pain behaviors and skin hypersensitivity in a model of bone cancer pain. Pain *157*, 1239–1247. https://doi.org/10.1097/j.pain.0000000000000514.

Guo, A., Vulchanova, L., Wang, J., Li, X., and Elde, R. (1999). Immunocytochemical localization of the vanilloid receptor 1 (VR1): relationship to neuropeptides, the P2X3 purinoceptor and IB4 binding sites. Eur. J. Neurosci. *11*, 946–958. https://doi.org/10.1046/j.1460-9568.1999.00503.x.

Guo, C., Liu, S., and Sun, M.Z. (2013). Novel insight into the role of GAPDH playing in tumor. Clin. Transl. Oncol. *15*, 167–172. https://doi.org/10.1007/s12094-012-0924-x.

Hamelin, V., Letourneux, C., Romeo, P.H., Porteu, F., and Gaudry, M. (2006). Thrombopoietin regulates IEX-1 gene expression through ERK-induced AML1 phosphorylation. Blood *107*, 3106–3113. https://doi.org/10.1182/blood-2005-07-2953.

Hammarberg, H., Piehl, F., Cullheim, S., Fjell, J., Hökfelt, T., and Fried, K. (1996). GDNF mRNA in Schwann cells and DRG satellite cells after chronic sciatic nerve injury. Neuroreport *7*, 857–860. https://doi.org/10.1097/00001756-199603220-00004.

Hargreaves, K.D.R., Brown, F., Flores, C., and Joris, J. (1988). A new and sensitive method for measuring thermal nociception in cutaneous hyperalgesia. Pain *32*, 77–88.

Hayashi, H., Ichihara, M., Iwashita, T., Murakami, H., Shimono, Y., Kawai, K., Kurokawa, K., Murakumo, Y., Imai, T., Funahashi, H., et al. (2000). Characterization of intracellular signals via tyrosine 1062 in RET activated by glial cell line-derived neurotrophic factor. Oncogene *19*, 4469–4475. https://doi.org/10.1038/sj.onc.1203799.

He, D.D., Gao, Y., Wang, S., Xie, Z., and Song, X.J. (2020a). Systematic administration of B vitamins alleviates diabetic pain and inhibits associated expression of P2X3 and TRPV1 in dorsal root ganglion neurons and proinflammatory cytokines in spinal cord in rats. Pain Res. Manag. *2020*, 3740162. https://doi.org/10.1155/2020/3740162.

He, J.J., Wang, X., Liang, C., Yao, X., Zhang, Z.S., Yang, R.H., and Fang, D. (2020b). Wnt5b/Ryk-mediated membrane trafficking of P2X3 receptors contributes to bone cancer pain. Exp. Neurol. *334*, 113482. https://doi.org/10.1016/j.expneurol.2020.113482.

Hu, S., Sun, Q., Du, W.J., Song, J., Li, X., Zhang, P.A., Xu, J.T., and Xu, G.Y. (2020). Adult stress promotes purinergic signaling to induce visceral pain in rats with neonatal maternal deprivation. Neurosci. Bull. *36*, 1271–1280. https://doi.org/10.1007/s12264-020-00575-7.

Huang, Z.J., and Song, X.J. (2008). Differing alterations of sodium currents in small dorsal root ganglion neurons after ganglion compression and peripheral nerve injury. Mol. Pain *4*, 20. https://doi.org/10.1186/1744-8069-4-20.

Ito, Y. (1999). Molecular basis of tissue-specific gene expression mediated by the runt domain transcription factor PEBP2/CBF. Gene Cell. *4*, 685–696. https://doi.org/10.1046/j.1365-2443.1999.00298.x.

Ito, Y., Bae, S.C., and Chuang, L.S.H. (2015). The RUNX family: developmental regulators in cancer. Nat. Rev. Cancer *15*, 81–95. https://doi.org/10.1038/nrc3877.

Ivanusic, J.J. (2009). Size, neurochemistry, and segmental distribution of sensory neurons innervating the rat tibia. J. Comp. Neurol. *517*, 276–283. https://doi.org/10.1002/cne.22160.

Jiang, H., Liu, J.P., Xi, K., Liu, L.Y., Kong, L.Y., Cai, J., Cai, S.Q., Han, X.Y., Song, J.G., Yang, X.M., et al. (2021). Contribution of AMPA receptor-mediated LTD in LA/BLA-CeA pathway to comorbid aversive and depressive symptoms in neuropathic pain. J. Neurosci. *41*, 7278–7299. https://doi.org/10.1523/jneurosci.2678-20.2021.

Jimenez-Andrade, J.M., Bloom, A.P., Stake, J.I., Mantyh, W.G., Taylor, R.N., Freeman, K.T., Ghilardi, J.R., Kuskowski, M.A., and Mantyh, P.W. (2010). Pathological sprouting of adult nociceptors in chronic prostate cancer-induced bone pain. J. Neurosci. *30*, 14649–14656. https://doi.org/10.1523/jneurosci.3300-10.2010.

Jørgensen, N.R. (2019). Role of the purinergic P2X receptors in osteoclast pathophysiology. Curr. Opin. Pharmacol. *47*, 97–101. https://doi.org/10.1016/j.coph.2019.02.013.

Kanaykina, N., Abelson, K., King, D., Liakhovitskaia, A., Schreiner, S., Wegner, M., and Kozlova, E.N. (2010). In vitro and in vivo effects on neural crest stem cell differentiation by conditional activation of Runx1 short isoform and its effect on neuropathic pain behavior. Ups. J. Med. Sci. *115*, 56–64. https://doi.org/10.3109/03009730903572065.

Kanno, T., Kanno, Y., Chen, L.F., Ogawa, E., Kim, W.Y., and Ito, Y. (1998). Intrinsic transcriptional activation-inhibition domains of the polyomavirus enhancer binding protein 2/core binding factor alpha subunit revealed in the presence of the beta subunit. Mol. Cell Biol. *18*, 2444–2454. https://doi.org/10.1128/mcb.18.5.2444.

Kashiba, H., Hyon, B., and Senba, E. (1998). Glial cell line-derived neurotrophic factor and nerve growth factor receptor mRNAs are expressed in distinct subgroups of dorsal root ganglion neurons and are differentially regulated by peripheral axotomy in the rat. Neurosci. Lett. *252*, 107–110. https://doi.org/10.1016/s0304-3940(98)00558-8.

Kawai, K., and Takahashi, M. (2020). Intracellular RET signaling pathways activated by GDNF. Cell Tissue Res. *382*, 113–123. https://doi.org/10.1007/s00441-020-03262-1.

Keast, J.R., Forrest, S.L., and Osborne, P.B. (2010). Sciatic nerve injury in adult rats causes distinct changes in the central projections of sensory neurons expressing different glial cell line-derived neurotrophic factor family receptors. J. Comp. Neurol. *518*, 3024–3045. https://doi.org/10.1002/cne.22378.

Kim, D.J., Khoury-Hanold, W., Jain, P.C., Klein, J., Kong, Y., Pope, S.D., Ge, W., Medzhitov, R., and Iwasaki, A. (2020). RUNX binding sites are enriched in herpesvirus genomes, and RUNX1 overexpression leads to herpes simplex virus 1 suppression. J. Virol. *94*, e00943-20. https://doi.org/10.1128/jvi.00943-20.

Kobayashi, A., Senzaki, K., Ozaki, S., Yoshikawa, M., and Shiga, T. (2012). Runx1 promotes neuronal differentiation in dorsal root ganglion. Mol. Cell. Neurosci. *49*, 23–31. https://doi.org/10.1016/j.mcn.2011.08.009.

Kobayashi, K., Fukuoka, T., Yamanaka, H., Dai, Y., Obata, K., Tokunaga, A., and Noguchi, K. (2005). Differential expression patterns of mRNAs for P2X receptor subunits in neurochemically characterized dorsal root ganglion neurons in the rat. J. Comp. Neurol. *481*, 377–390. https://doi.org/10.1002/cne.20393.

Krajewski, J.L. (2020). P2X3-Containing receptors as targets for the treatment of chronic pain. Neurotherapeutics *17*, 826–838. https://doi.org/10.1007/s13311-020-00934-2.

Kramer, I., Sigrist, M., de Nooij, J.C., Taniuchi, I., Jessell, T.M., and Arber, S. (2006). A role for Runx transcription factor signaling in dorsal root ganglion sensory neuron diversification. Neuron *49*, 379–393. https://doi.org/10.1016/j.neuron.2006.01.008.

Kucharczyk, M.W., Chisholm, K.I., Denk, F., Dickenson, A.H., Bannister, K., and McMahon, S.B. (2020). The impact of bone cancer on the peripheral encoding of mechanical pressure stimuli. Pain *161*, 1894–1905. https://doi.org/10.1097/j.pain.0000000000001880.

Kurtzeborn, K., Kwon, H.N., and Kuure, S. (2019). MAPK/ERK signaling in regulation of renal differentiation. Int. J. Mol. Sci. *20*, E1779. https://doi.org/10.3390/ijms20071779.

Li, G., Ma, F., Gu, Y., and Huang, L.Y.M. (2013). Analgesic tolerance of opioid agonists in mutant mu-opioid receptors expressed in sensory neurons following intrathecal plasmid gene delivery. Mol. Pain *9*, 63. https://doi.org/10.1186/1744-8069-9-63.

Lie, A.L.M., Mevel, R., Patel, R., Blyth, K., Baena, E., Kouskoff, V., and Lacaud, G. (2020). RUNX1 dosage in development and cancer. Mol. Cells *43*, 126–138. https://doi.org/10.14348/molcells.2019.0301.

Liepe, K., Geidel, H., Haase, M., Hakenberg, O.W., Runge, R., and Kotzerke, J. (2005). New model for the induction of osteoblastic bone metastases in rat. Anticancer Res. *25*, 1067–1073.

Lindsay, T.H., Jonas, B.M., Sevcik, M.A., Kubota, K., Halvorson, K.G., Ghilardi, J.R., Kuskowski, M.A., Stelow, E.B., Mukherjee, P., Gendler, S.J., et al. (2005). Pancreatic cancer pain and its correlation with changes in tumor vasculature, macrophage infiltration, neuronal innervation, body weight and disease progression. Pain *119*, 233–246. https://doi.org/10.1016/j.pain.2005.10.019.

Liu, K., Tang, Z., Huang, A., Chen, P., Liu, P., Yang, J., Lu, W., Liao, J., Sun, Y., Wen, S., et al. (2017). Glyceraldehyde-3-phosphate dehydrogenase promotes cancer growth and metastasis through upregulation of SNAIL expression. Int. J. Oncol. *50*, 252–262. https://doi.org/10.3892/ijo.2016.3774.

Liu, M., Liu, Y., Hou, B., Bu, D., Shi, L., Gu, X., and Ma, Z. (2015). Kinesin superfamily protein 17 contributes to the development of bone cancer pain by participating in NR2B transport in the spinal cord of mice. Oncol. Rep. *33*, 1365–1371. https://doi.org/10.3892/or.2015.3706.

Liu, M., Yang, H., Fang, D., Yang, J.J., Cai, J., Wan, Y., Chui, D.H., Han, J.S., and Xing, G.G. (2013). Upregulation of P2X3 receptors by neuronal calcium sensor protein VILIP-1 in dorsal root ganglions contributes to the bone cancer pain in rats. Pain *154*, 1551–1568. https://doi.org/10.1016/j.pain.2013.04.022.

Malin, S.A., Molliver, D.C., Koerber, H.R., Cornuet, P., Frye, R., Albers, K.M., and Davis, B.M. (2006). Glial cell line-derived neurotrophic factor family members sensitize nociceptors in vitro and produce thermal hyperalgesia in vivo. J. Neurosci. *26*, 8588–8599. https://doi.org/10.1523/jneurosci.1726-06.2006.

Mantyh, P. (2013). Bone cancer pain: causes, consequences, and therapeutic opportunities. Pain *154*, S54–S62. https://doi.org/10.1016/j.pain.2013.07.044.

Mantyh, P.W. (2019). Mechanisms that drive bone pain across the lifespan. Br. J. Clin. Pharmacol. *85*, 1103–1113. https://doi.org/10.1111/bcp.13801.

Mantyh, W.G., Jimenez-Andrade, J.M., Stake, J.I., Bloom, A.P., Kaczmarska, M.J., Taylor, R.N., Freeman, K.T., Ghilardi, J.R., Kuskowski, M.A., and Mantyh, P.W. (2010). Blockade of nerve sprouting and neuroma formation markedly attenuates the development of late stage cancer pain. Neuroscience *171*, 588–598. https://doi.org/10.1016/j.neuroscience.2010.08.056.

Marmigère, F., Montelius, A., Wegner, M., Groner, Y., Reichardt, L.F., and Ernfors, P. (2006). The Runx1/AML1 transcription factor selectively regulates development and survival of TrkA nociceptive sensory neurons. Nat. Neurosci. *9*, 180–187. https://doi.org/10.1038/nn1631.

McGaraughty, S., Wismer, C.T., Zhu, C.Z., Mikusa, J., Honore, P., Chu, K.L., Lee, C.H., Faltynek, C.R., and Jarvis, M.F. (2003). Effects of A-317491, a novel and selective P2X3/P2X2/3 receptor antagonist, on neuropathic, inflammatory and chemogenic nociception following intrathecal and intraplantar administration. Br. J. Pharmacol. *140*, 1381–1388. https://doi.org/10.1038/sj.bjp.0705574.

Medhurst, S.J., Walker, K., Bowes, M., Kidd, B.L., Glatt, M., Muller, M., Hattenberger, M., Vaxelaire, J., O'Reilly, T., Wotherspoon, G., et al. (2002). A rat model of bone cancer pain. Pain *96*, 129–140. https://doi.org/10.1016/s0304-3959(01)00437-7.

Meng, F.F., Xu, Y., Dan, Q.Q., Wei, L., Deng, Y.J., Liu, J., He, M., Liu, W., Xia, Q.J., Zhou, F.H., et al. (2015). Intrathecal injection of lentivirus-mediated glial cell line-derived neurotrophic factor RNA interference relieves bone cancer-induced pain in rats. Cancer Sci. *106*, 430–437. https://doi.org/10.1111/cas.12609.

Natura, G., von Banchet, G.S., and Schaible, H.G. (2005). Calcitonin gene-related peptide enhances TTX-resistant sodium currents in cultured dorsal root ganglion neurons from adult rats. Pain *116*, 194–204. https://doi.org/10.1016/j.pain.2005.04.002.

Nencini, S., Ringuet, M., Kim, D.H., Greenhill, C., and Ivanusic, J.J. (2018). GDNF, neurturin, and artemin activate and sensitize bone afferent neurons and contribute to inflammatory bone pain. J. Neurosci. *38*, 4899–4911. https://doi.org/10.1523/jneurosci.0421-18.2018.

Nunez-Badinez, P., Sepúlveda, H., Diaz, E., Greffrath, W., Treede, R.D., Stehberg, J., Montecino, M., and van Zundert, B. (2018). Variable transcriptional responsiveness of the P2X3 receptor gene during CFA-induced inflammatory hyperalgesia. J. Cell. Biochem. *119*, 3922–3935. https://doi.org/10.1002/jcb.26534.

Ohta, K., Inokuchi, T., Gen, E., and Chang, J. (2001). Ultrastructural study of anterograde transport of glial cell line-derived neurotrophic factor from dorsal root ganglion neurons of rats towards the nerve terminal. Cells Tissues Organs *169*, 410–421. https://doi.org/10.1159/000047909.

Petruska, J.C., Cooper, B.Y., Johnson, R.D., and Gu, J.G. (2000). Distribution patterns of different P2x receptor phenotypes in acutely dissociated dorsal root ganglion neurons of adult rats. Exp. Brain Res. *134*, 126–132. https://doi.org/10.1007/s002210000414.

Plaza-Menacho, I., Burzynski, G.M., de Groot, J.W., Eggen, B.J.L., and Hofstra, R.M.W. (2006). Current concepts in RET-related genetics, signaling and therapeutics. Trends Genet. *22*, 627–636. https://doi.org/10.1016/j.tig.2006.09.005.

Price, T.J., and Flores, C.M. (2007). Critical evaluation of the colocalization between calcitonin gene-related peptide, substance P, transient receptor potential vanilloid subfamily type 1 immunoreactivities, and isolectin B4 binding in primary afferent neurons of the rat and mouse. J. Pain *8*, 263–272. https://doi.org/10.1016/j.jpain.2006.09.005.

Qiao, W.L., Li, Q., Hao, J.W., Wei, S., Li, X.M., Liu, T.T., Qiu, C.Y., and Hu, W.P. (2022). Enhancement of P2X3 receptor-mediated currents by lysophosphatidic acid in rat primary sensory neurons. Front. Pharmacol. *13*, 928647. https://doi.org/10.3389/fphar.2022.928647.

Qu, X.X., Cai, J., Li, M.J., Chi, Y.N., Liao, F.F., Liu, F.Y., Wan, Y., Han, J.S., and Xing, G.G. (2009). Role of the spinal cord NR2B-containing NMDA receptors in the development of neuropathic pain. Exp. Neurol. *215*, 298–307. https://doi.org/10.1016/j.expneurol.2008.10.018.

Ramer, M.S., Bradbury, E.J., and McMahon, S.B. (2001). Nerve growth factor induces P2X(3) expression in sensory neurons. J. Neurochem. *77*, 864–875. https://doi.org/10.1046/j.1471-4159.2001.00288.x.

Rind, H.B., and von Bartheld, C.S. (2002). Anterograde axonal transport of internalized GDNF in sensory and motor neurons. Neuroreport *13*, 659–664. https://doi.org/10.1097/00001756-200204160-00025.

Rivlin, A.S., and Tator, C.H. (1977). Objective clinical assessment of motor function after experimental spinal cord injury in the rat. J. Neurosurg. *47*, 577–581. https://doi.org/10.3171/jns.1977.47.4.0577.

Robertson, S.J., Rae, M.G., Rowan, E.G., and Kennedy, C. (1996). Characterization of a P2X-purinoceptor in cultured neurones of the rat dorsal root ganglia. Br. J. Pharmacol. *118*, 951–956. https://doi.org/10.1111/j.1476-5381.1996.tb15491.x.

Ruan, H.Z., Birder, L.A., de Groat, W.C., Tai, C., Roppolo, J., Buffington, C.A., and Burnstock, G. (2005). Localization of P2X and P2Y receptors in dorsal root ganglia of the cat. J. Histochem.

Cytochem. *53*, 1273–1282. https://doi.org/10.1369/jhc.4A6556.2005.

Rumney, R.M.H., Wang, N., Agrawal, A., and Gartland, A. (2012). Purinergic signalling in bone. Front. Endocrinol. *3*, 116. https://doi.org/10.3389/fendo.2012.00116.

Salio, C., Aimar, P., Malapert, P., Moqrich, A., and Merighi, A. (2021). Neurochemical and ultrastructural characterization of unmyelinated non-peptidergic C-nociceptors and C-low threshold mechanoreceptors projecting to lamina II of the mouse spinal cord. Cell. Mol. Neurobiol. *41*, 247–262. https://doi.org/10.1007/s10571-020-00847-w.

Sato, M., Sato, T., Yajima, T., Shimazaki, K., and Ichikawa, H. (2018). The transient receptor potential cation channel subfamily V members 1 and 2, P2X purinoceptor 3 and calcitonin gene-related peptide in sensory neurons of the rat trigeminal ganglion, innervating the periosteum, masseter muscle and facial skin. Arch. Oral Biol. *96*, 66–73. https://doi.org/10.1016/j.archoralbio.2018.08.012.

Shiers, S.I., Sankaranarayanan, I., Jeevakumar, V., Cervantes, A., Reese, J.C., and Price, T.J. (2021). Convergence of peptidergic and non-peptidergic protein markers in the human dorsal root ganglion and spinal dorsal horn. J. Comp. Neurol. *529*, 2771–2788. https://doi.org/10.1002/cne.25122.

Shin, D.S., Kim, E.H., Song, K.Y., Hong, H.J., Kong, M.H., and Hwang, S.J. (2008). Neurochemical characterization of the TRPV1-positive nociceptive primary afferents innervating skeletal muscles in the rats. J. Korean Neurosurg. Soc. *43*, 97–104. https://doi.org/10.3340/jkns.2008.43.2.97.

Surprenant, A., and North, R.A. (2009). Signaling at purinergic P2X receptors. Annu. Rev. Physiol. *71*, 333–359. https://doi.org/10.1146/annurev.physiol.70.113006.100630.

Swett, J.E., Torigoe, Y., Elie, V.R., Bourassa, C.M., and Miller, P.G. (1991). Sensory neurons of the rat sciatic nerve. Exp. Neurol. *114*, 82–103. https://doi.org/10.1016/0014-4886(91)90087-s.

Takahashi, M. (2001). The GDNF/RET signaling pathway and human diseases. Cytokine Growth Factor Rev. *12*, 361–373. https://doi.org/10.1016/s1359-6101(01)00012-0.

Tang, Z., Yuan, S., Hu, Y., Zhang, H., Wu, W., Zeng, Z., Yang, J., Yun, J., Xu, R., and Huang, P. (2012). Over-expression of GAPDH in human colorectal carcinoma as a preferred target of 3-bromopyruvate propyl ester. J. Bioenerg. Biomembr. *44*, 117–125. https://doi.org/10.1007/s10863-012-9420-9.

Ueno, S., Tsuda, M., Iwanaga, T., and Inoue, K. (1999). Cell type-specific ATP-activated responses in rat dorsal root ganglion neurons. Br. J. Pharmacol. *126*, 429–436. https://doi.org/10.1038/sj.bjp.0702319.

Ugarte, G.D., Opazo, T., Leisewitz, F., van Zundert, B., and Montecino, M. (2012). Runx1 and C/EBPbeta transcription factors directly up-regulate P2X3 gene transcription. J. Cell. Physiol. *227*, 1645–1652. https://doi.org/10.1002/jcp.22882.

Urch, E.C., Donovan-Rodriguez, T., and Dickenson, H.A. (2003). Alterations in dorsal horn neurones in a rat model of cancer-induced bone pain. Pain *106*, 347–356. https://doi.org/10.1016/j.pain.2003.08.002.

Vandesompele, J., De Preter, K., Pattyn, F., Poppe, B., Van Roy, N., De Paepe, A., and Speleman, F. (2002). Accurate normalization of real-time quantitative RT-PCR data by geometric averaging of multiple internal control genes. Genome Biol. *3*. RESEARCH0034. https://doi.org/10.1186/gb-2002-3-7-research0034.

Vilceanu, D., Honore, P., Hogan, Q.H., and Stucky, C.L. (2010). Spinal nerve ligation in mouse upregulates TRPV1 heat function in injured IB4-positive nociceptors. J. Pain *11*, 588–599. https://doi.org/10.1016/j.jpain.2009.09.018.

Wacnik, P.W., Eikmeier, L.J., Ruggles, T.R., Ramnaraine, M.L., Walcheck, B.K., Beitz, A.J., and Wilcox, G.L. (2001). Functional interactions between tumor and peripheral nerve: morphology, algogen identification, and behavioral characterization of a new murine model of cancer pain. J. Neurosci. *21*, 9355–9366. https://doi.org/10.1523/jneurosci.21-23-09355.2001.

Wirkner, K., Sperlagh, B., and Illes, P. (2007). P2X3 receptor involvement in pain states. Mol. Neurobiol. *36*, 165–183. https://doi.org/10.1007/s12035-007-0033-y.

Wu, J.X., Xu, M.Y., Miao, X.R., Lu, Z.J., Yuan, X.M., Li, X.Q., and Yu, W.F. (2012). Functional up-regulation of P2X3 receptors in dorsal root ganglion in a rat model of bone cancer pain. Eur. J. Pain *16*, 1378–1388. https://doi.org/10.1002/j.1532-2149.2012.00149.x.

Xiang, Z., Xiong, Y., Yan, N., Li, X., Mao, Y., Ni, X., He, C., LaMotte, R.H., Burnstock, G., and Sun, J. (2008). Functional up-regulation of P2X 3 receptors in the chronically compressed dorsal root ganglion. Pain *140*, 23–34. https://doi.org/10.1016/j.pain.2008.07.006.

Yang, Y., Li, S., Jin, Z.R., Jing, H.B., Zhao, H.Y., Liu, B.H., Liang, Y.J., Liu, L.Y., Cai, J., Wan, Y., and Xing, G.G. (2018). Decreased abundance of TRESK two-pore domain potassium channels in sensory neurons underlies the pain associated with bone metastasis. Sci. Signal. *11*, eaao5150. https://doi.org/10.1126/scisignal.aao5150.

Yi, S., Kim, J., and Lee, S.Y. (2020). GDNF secreted by pre-osteoclasts induces migration of bone marrow mesenchymal stem cells and stimulates osteogenesis. BMB Rep. *53*, 646–651. https://doi.org/10.5483/BMBRep.2020.53.12.199.

Yoshikawa, M., Senzaki, K., Yokomizo, T., Takahashi, S., Ozaki, S., and Shiga, T. (2007). Runx1 selectively regulates cell fate specification and axonal projections of dorsal root ganglion neurons. Dev. Biol. *303*, 663–674. https://doi.org/10.1016/j.ydbio.2006.12.007.

Yu, J., Du, J., Fang, J., Liu, Y., Xiang, X., Liang, Y., Shao, X., and Fang, J. (2021). The interaction between P2X3 and TRPV1 in the dorsal root ganglia of adult rats with different pathological pains. Mol. Pain *17*. 17448069211011315. https://doi.org/10.1177/17448069211011315.

Zheng, J. (2012). Energy metabolism of cancer: glycolysis versus oxidative phosphorylation (Review). Oncol. Lett. *4*, 1151–1157. https://doi.org/10.3892/ol.2012.928.

Zheng, Q., Fang, D., Cai, J., Wan, Y., Han, J.S., and Xing, G.G. (2012). Enhanced excitability of small dorsal root ganglion neurons in rats with bone cancer pain. Mol. Pain *8*, 24. https://doi.org/10.1186/1744-8069-8-24.

Zheng, Q., Fang, D., Liu, M., Cai, J., Wan, Y., Han, J.S., and Xing, G.G. (2013). Suppression of KCNQ/M (Kv7) potassium channels in dorsal root ganglion neurons contributes to the development of bone cancer pain in a rat model. Pain *154*, 434–448. https://doi.org/10.1016/j.pain.2012.12.005.

Zhong, Z., Chen, A., Fa, Z., Ding, Z., Xiao, L., Wu, G., Wang, Q., and Zhang, R. (2020). Bone marrow mesenchymal stem cells upregulate PI3K/AKT pathway and down-regulate NF-κB pathway by secreting glial cell-derived neurotrophic factors to regulate microglial polarization and alleviate deafferentation pain in rats. Neurobiol. Dis. *143*, 104945. https://doi.org/10.1016/j.nbd.2020.104945.

Zhou, Y.L., Jiang, G.Q., Wei, J., Zhang, H.H., Chen, W., Zhu, H., Hu, S., Jiang, X., and Xu, G.Y. (2015). Enhanced binding capability of nuclear factor-kappaB with demethylated P2X3 receptor gene contributes to cancer pain in rats. Pain *156*, 1892–1905. https://doi.org/10.1097/j.pain.0000000000000248.

Zimmermann, M. (1983). Ethical guidelines for investigations of experimental pain in conscious animals. Pain *16*, 109–110. https://doi.org/10.1016/0304-3959(83)90201-4.

Zimmermann, M. (2001). Pathobiology of neuropathic pain. Eur. J. Pharmacol. *429*, 23–37. https://doi.org/10.1016/s0014-2999(01)01303-6.

STAR★METHODS

KEY RESOURCES TABLE

REAGENT or RESOURCE	SOURCE	IDENTIFIER
Antibodies		
Guinea pig anti-P2X3R (for Immunofluorescence staining)	Novus	Cat# NB100-1658
Mouse anti-rat CGRP	Abcam	Cat# ab23981
Mouse anti-pig NF200	Sigma-Aldrich	Cat#N0142
Rabbit anti-rat P2X3R (for Western blot)	Alomone labs	Cat# APR-016
Rabbit anti-mouse Runx1 (for Immunofluorescence staining)	Abcam	Cat# ab23980
Rabbit anti-pRunx1^{Ser249}	Cell Signaling Technology	Cat# 4327S
Rabbit anti-Runx1 (for Western blot)	Abcam	Cat# ab272456
Mouse anti-β-actin	CVV-BIO	Cat# CW0096M
Rabbit anti-pERK1/2	Cell Signaling Technology	Cat# 4370S
Rabbit anti-ERK1/2	Cell Signaling Technology	Cat# 4695S
Mouse anti-GFRα1	Santa Cruz Biotechnology	Cat#sc-271546
Mouse anti-GAPDH	ZSGB-Bio	Cat# TA-08
Anti-GDNF antibody	Abcam	Cat# ab28956
FITC-conjugated Bandeiraea simplicifolia IB4 (IHC)	Sigma-Aldrich	Cat# L2895
Goat anti-rabbit IgG (H&L)	ZSGB-Bio	Cat# ZDR-5306
Goat anti-mouse IgG (H&L)	ZSGB-Bio	Cat# ZDR-2305
Alexa Fluor 647 donkey anti-guinea pig IgG	Jackson Immuno Research	Cat# 706-606-148
Donkey polyclonal anti-rabbit Cy3	Jackson Immuno Research	Cat# 711-165-152
Bacterial and virus strains		
Lentivirus-expressing GFP	Obio Technology	N/A
Lentivirus-expressing Runx1-GFP	Obio Technology	N/A
Chemicals, peptides, and recombinant proteins		
Recombinant human GDNF	R&D SYSTEM	Cat# 512-GF-01M
Pentobarbital sodium	Sigma-Aldrich	Cat# P3761
DMSO	Sigma-Aldrich	Cat# 276855; CAS: 67-68-5
PEG 300	MedChemExpress	Cat# 25322-68-3
α,β-meATP	Tocris Bioscience	Cat# 3209
RPI-1	Merck Biosciences	Cat# 269730-03-2
PD98059	Merck Biosciences	Cat# 167869-21-8
LY294002	Merck Biosciences	Cat# 934389-88-5
PP2	Merck Biosciences	Cat#172889-27-9
Anisomycin	Merck Biosciences	Cat# 22862-76-6
SCH772984	Selleck	Cat# S7101
Poly-d-lysine (PDL)	Sigma-Aldrich	Cat# P0899
Fetal bovine serum (FBS)	ScienProCell	Cat# FBS-SPC900A
Dulbecco's modified Eagle's medium (DMEM)	Gibco	Cat# 12100046
Collagenasetype IA	Sigma-Aldrich	Cat# C9891

(*Continued on next page*)

Continued

REAGENT or RESOURCE	SOURCE	IDENTIFIER
Trypsintype II-S	Sigma-Aldrich	Cat# T7409
Neurobasal growth medium	Gibco	Cat# 21103049
B27	Gibco	Cat# 17504044
Glutamax	Sigma-Aldrich	Cat# G7513
Penicillin	Beyotime Biotechnology	Cat# C0222
Streptomycin	Beyotime Biotechnology	Cat# C0222
IB4	Sigma-Aldrich	Cat# L2895
4′,6-diamidino-2-phenylindole (DAPI)	Sigma-Aldrich	Cat# P3761
Runx1 siRNA	Invitrogen	Cat# 16708
Tat-Ser peptide (YGRKKRRQRRRMQDARQ IQPSPPWSYDQSY)	ChinaPeptides Co., Ltd.	N/A
Tat-Ala peptide (YGRKKRRQRRRMQDA RQIQPAPPWSYDQSY)	ChinaPeptides Co., Ltd.	N/A
Critical commercial assays		
BCA Protein Assay Kit	Pierce	Cat# 23227
Qick-Change-Site-Directed Mutagenesis Kit	Agilent Technologies, Santa Clara, CA	Cat# 200519
Protease inhibitor cocktail	Pierce	Cat# 78437
GDNF (rat) ELISA Kit (BDNF Emax ImmunoAssay System)	Promege	Cat# G7611
Lipofectamine® 2000 Transfection Reagent	Invitrogen	Cat# 11668
Experimental models: Cell lines		
MRMT-1 rat mammary gland tumor cells	Provided by Novartis Oncology Research, Basel.	N/A
PC12 cells	COBIOER BIOSCIENCES	CBP61026
SH-SY5Y cells	COBIOER BIOSCIENCES	CBP60913
Experimental models: Organisms/strains		
Rat: Sprague-Dawley	Charles River	N/A
Oligonucleotides		
GFRα1 antisense oligodeoxynucleotide (5′-TAGGAACATGGTGCC-3′), see Table S2	This paper	N/A
GFRα1 missense oligodeoxynucleotide (5′-TAGAGACTAGGTGCC-3′), see Table S2	This paper	N/A
Software and algorithms		
EPC-10 amplifier	HEKA	http://www.heka.com/products/products_main.html#physiol_epc10single
Patch-Master software	HEKA	http://www.heka.com/downloads/downloads_main.html#down_patchmaster
RSC-200 rapid solution changer system	Bio-Logic Science Instruments	https://www.biologic.net/products/rsc200/
MetaFluor v7	Molecular Devices	ccellular-imaging-systems/acquisition-and-analysis-software/metamorph-microscopy
Leica LAS X 3.0	Leica	https://www.leica-microsystems.com/products/microscope-software
GraphPad Prism 8.0	GraphPad Software	https://www.graphpad.com/scientific-software/

RESOURCE AVAILABILITY

Lead contact

Further information and requests for resources and reagents should be directed to and will be fulfilled by the lead contact, Dr. Guo-Gang Xing (ggxing@bjmu.edu.cn).

Materials availability

This study did not generate new unique reagents.

Data and code availability

- All data reported in this paper will be shared by the lead contact on request.
- This paper does not report original code.
- Any additional information required to reanalyze the data reported in this paper is available from the lead contact on request.

EXPERIMENTAL MODEL AND SUBJECT DETAILS

Animals

Adult female Sprague-Dawley rats weighing 180 to 220g at the beginning of the experiments were provided by the Department of Experimental Animal Sciences, Peking University Health Science Center, and were randomly assigned to experimental groups. All rats were housed in separated cages, and the room was kept at 24 ± 1°C and 50 to 60% humidity under a 12-hour light/12-hour dark cycle with *ad libitum* access to food and water. All animal experimental procedures were carried out in accordance with the guidelines of the International Association for the Study of Pain (Zimmermann, 1983) and were approved by the Animal Care and Use Committee of Peking University.

METHOD DETAILS

Plasmid construction, transient transfections and reporter assays

Empty vectors pGL3-basic, pRL-CMV and plasmid pcDNA3.1(+) were purchased from Promega (Promega, Madison, WI) and Invitrogen (Carlsbad, CA), respectively. Luciferase reporter constructs carrying either the full-length (1,934 bp) rat P2X3 gene promoter containing 6 putative consensus-binding sites for Runx1 (p1,934-P2X3-Luc) or 5′ deletions of this promoter containing R1 binding site of Runx1 (p415-P2X3-Luc), and mouse Runx1 expressing plasmids (pcDNA3.1-Runx1) were generously provided by Dr. Martin Montecino (University of Andres Bello, Santiago, Chile). Mutant version of p415-P2X3-Luc at R1 binding site of Runx1 (p415-P2X3-mu) and mutation of Runx1 serine sites 249/266 to either alanine (249/266A) or aspartic acid (249/266D) were generated with QuikChange-Site-Directed Mutagenesis Kit (Agilent Technologies, Santa Clara, CA), according with manufacturer's instructions. All these reporter vectors were confirmed by automatic sequencing.

Transfections of plasmids into PC12 cells or SH-SY5Y cells were carried out using Lipofectamine 2000 Transfection Reagent (Invitrogen, Carlsbad, CA) in 24-well plates, following the manufacturer's instructions. The cells were transfected with 200 ng of the Firefly luciferase reporter plasmids and 10 ng of the Renilla luciferase (pRL-SV-40) plasmid as internal control (Promega, Madison, WI). After 24 h, the cells were harvested using 50 μL of passive lysis buffer (Promega) per well. Cell lysates (20 μL) were evaluated for Firefly luciferase activity using the Dual-Luciferase Reporter Assay System (Promega) according to the manufacturer's instructions and normalized to values of Renilla luciferase activity (Ugarte et al., 2012). All transfections were normalized by co-expression of Renilla luciferase plasmid and displayed as relative luciferase units (RLU).

In some experiments (Figure 4), SH-SY5Y cells which were transfected with either p1,934-P2X3-Luc plasmids and pcDNA3.1-Runx1 plasmids (Runx1-wt), or p1,934-P2X3-Luc plasmids and pRunx1-mu (S249/266A, S249/266D) plasmids, were respectively treated with GDNF (100 ng/mL) for 24 h, or pretreated with PD98059 (20 μM, Merck Biosciences) for 30 min before GDNF (100 ng/mL) stimulation. Then, the cells were harvested and the luciferase activity was measured as abovementioned. See Table S1 and S2 for the use of plasmids and oligonucleotides sequences.

Animal model of bone cancer pain

Surgery

A rat model of bone cancer pain was established by intratibial injection of syngeneic MRMT-1 rat mammary gland tumor cells according to the methods described in previous reports (Liu et al., 2013; Medhurst et al., 2002; Yang et al., 2018). Briefly, after being anesthetized with 1% pentobarbital sodium [0.05 g/kg, intraperitoneal (i.p.)], the left tibia of rat was carefully exposed and a 23-gauge needle was inserted in the canal of the bone. It was then removed and replaced with a long, thin blunt needle attached to a 10-μL Hamilton syringe containing the medium to be injected. A volume of 4 μL MRMT-1 rat mammary gland tumor cells (4×10^4) or vehicle (PBS) was injected into the tibial bone cavity. After injection, the site was sealed with bone wax, and the wound was finally closed. Any rats exhibiting motor deficiency or lack of pain hypersensitivity at 14 days after tumor cell inoculation, as well as those that died during the experiments, were excluded from the study.

Bone radiological detection

To assess the bone destruction after tumor cells inoculation, tibia bone radiographs were performed in this study. On days 14 and 21 after tumor cells inoculation, tibial bone radiographs from both hind limbs of PBS- and MRMT-1-treated rats (n = 4 for each group) were taken by using a Digital Radiographer System (DR7000, Eastman Kodak Company, USA). Radiographic images of the tibia bones were assessed for extent of destruction as previously described (Urch et al., 2003; Zheng et al., 2013).

Intrathecal catheterization

Intrathecal catheterization is a reliable approach for the delivery of drugs into the DRG of animals for the long-lasting behavioral and pharmacological studies (Li et al., 2013; Yang et al., 2018). Under general anesthesia via intraperitoneal injection (i.p.) of pentobarbital sodium (50 mg/kg), implantation of an intrathecal catheter was performed as described in previous studies (Qu et al., 2009; Yang et al., 2018). Briefly, a PE-10 polyethylene catheter was implanted between the L5 and L6 vertebrae to reach the lumbar enlargement of the spinal cord. The outer part of the catheter was plugged and fixed onto the skin upon closure of the wound. All surgical procedures were performed under sterile conditions. Rats showing neurological deficits after the catheter implantation were euthanized. After recovery for 3 to 7 days, drugs or vectors were intrathecally injected via the implanted catheter in a 10-μL volume of solution (for lentivirus injection, 20 μL) followed by 10 μL of vehicle for flushing. Each injection lasted for at least 5 min. After an injection, the needle remained *in situ* for 2 min before being withdrawn.

Drug administration and lentivirus infection

Runx1 siRNA (2.5 μg) or an equal dose of scramble siRNA in a 10-μL mixture with *in vivo* jetPEI transfection reagent (Polyplus-transfection SA, Illkirch, France) was intrathecally administered to the tumor-bearing rats once every two days for three times, on day 7 after tumor cells inoculation (See Figure 2). Construction and production of recombinant lentivirus expressing Runx1 linked with GFP (LV-Runx1) were completed by Obio Technology (Shanghai, China) using pLVX-mCMV-GFP vector. Lentivirus, including LV-Runx1 and its control LV-GFP, was intrathecally administered to rats at a final titer of 5×10^8 transducing units/mL (in a 20-μL volume of solution), respectively. The lentivirus was intrathecally delivered to animals on day 7 after intrathecal catheterization surgery in naïve rats (See Figure 3). Recombinant human GDNF (200 ng in a 10-μL volume) or vehicle was intrathecally administered to the naïve rats once per day for four consecutive days (See Figure 5). In some experiments, SCH772984 (15 μM × 10 μL), or alternatively, Runx1 siRNA or scramble siRNA (2.5 μg in a 10-μL volume), was intrathecally administered to the naïve rats at one hour before GDNF application (See Figure S2). In tumor-bearing rats, both GFRα1-AS ODN (at a dose of 30 μg dissolved in 10 μL of nuclease-free normal saline) and mismatched ODNs, respectively, were intrathecally administered to bone metastasis model rats on day 7 after tumor cells inoculation, once per day for seven consecutive days (See Figure 6). In some experiments, SCH772984 (15 μM × 10 μL) or vehicle was intrathecally administered to tumor-bearing rats on day 10 after tumor cells inoculation, twice per day for four consecutive days (See Figure 7). Although in other experiments, interfering peptide TAT-Ser (YGRKKRRQRRRMQDARQIQPSPPWSYDQSY) or its control peptide TAT-Ala (YGRKKRRQRRRMQD ARQIQPAPPWSYDQSY) was intrathecally injected to bone metastasis model rats by osmotic pump (25 ng per rat) for seven consecutive days, on day 7 after tumor cells inoculation (See Figure S3). See Table S2 for the use of Runx1 siRNA and GFRα1 antisense oligodeoxynucleotide.

Behavioral tests

Animals were placed in individual plastic boxes and allowed to acclimate for 30 min before the behavioral testing. All behavioral experiments thereafter were performed in a blinded fashion (the tester was blinded to treatment groups). Animals were randomly placed into treatment groups with 8 to 15 rats per treatment group per trial in consideration of the excluded ones, and the number for statistical analysis did not include the excluded rats.

Mechanical hypersensitivity, as a behavioral sign of bone cancer pain, was assessed by measuring 50% paw withdrawal threshold (PWT) as described in our previous reports (Jiang et al., 2021; Yang et al., 2018). The 50% PWT in response to a series of von Frey filament (Stoelting, Wood Dale, IL) was determined by the up-and-down method (Chaplan et al., 1994). Eight von Frey filaments with about equal logarithmic incremental (0.224) bending forces were chosen (0.41g, 0.70g, 1.20g, 2.00g, 3.63g, 5.50g, 8.50g, and 15.10g). The 50% PWT was calculated using the following formula: 50% PWT (g) = $10^{[X_f+\kappa\delta]}$, where X_f is the value of the final von Frey filament used (in log units), κ is a value measured from the pattern of positive/negative response, and $\delta = 0.224$, which is the average interval (in log units) between the von Frey filaments. If an animal did not respond to the highest von Frey filament, then the value was recorded as 15.10 g. In rats, the mechanical hypersensitivity is assessed by measuring the 50% PWT to von Frey filaments, and an allodynic rat is defined as that whose 50% PWT is less than 4.0 g (i.e., withdrawal in response to non-noxious tactile stimulus) (Zimmermann, 2001).

Thermal hyperalgesia of the hind paws was tested according the methods described by Hargreaves (Hargreaves et al., 1988). Rats were allowed to acclimate for a minimum of 30 min before testing. A radiant heat source was focused onto the plantar surface of the hind paw. Measurements of paw withdrawal latency (PWL) were taken by a timer that was started by the activation of the heat source and stopped when withdrawal of the paw was detected with a photodetector. A maximal cutoff time of 30 s was used to prevent unnecessary tissue damage. Three measurements of PWL were taken for each hind paw and were averaged as the result of each test session. The hind paw was tested alternately with >5-min intervals between consecutive tests.

Spontaneous pain-related behaviors were recorded as described elsewhere (Yang et al., 2018). Flinching and guarding were observed for 10 min during a resting state after a 30-min acclimation period. Flinching was defined as the lifting and rapid flexing of the ipsilateral hind paw not associated with walking or movement. The number of flinches was recorded within the 10-min observation period. Guarding was characterized by fully retracting the ipsilateral hind limb under the torso. The time the hind paw was retracted during the 10-min period was recorded. Studies were performed in a blinded manner (the observer was blinded to all treatments).

Locomotor function was assessed with the inclined plate test, according to the method reported by Rivlin and Tator (1977). Briefly, animals were placed crosswise to the long axis of an inclined plate. The initial angle of the inclined plate was 50°. The angle was then adjusted in 5° increments. The maximum angle of the plate on which the rat maintained its body position for 5 s without falling was determined. In this study, the inclined plate test was performed for all behavioral experiments in which the animals received intrathecal drugs.

Primary culture and acute dissociation of DRG neurons

Primary cultures of DRG neurons were performed according to the method described in previous study (Natura et al., 2005). Briefly, rats (2 weeks old) were euthanized with ether, and DRGs were dissected from the lumbar spinal segments. The ganglia were digested with collagenase type IA (3 mg/mL; Sigma) for 50 min and 0.25% trypsin (type II-S, Sigma-Aldrich) for another 10 min at 37°C. After terminating the enzymatic treatment by Dulbecco's modified Eagle's medium (DMEM) plus 10% fetal bovine serum, ganglia were dissociated with a polished Pasteur pipette, and the suspension of ganglia was sieved through a filter to remove debris and centrifuged at 800 rpm for 2 min. The resuspended cells were plated on 35-mm dishes coated with poly-D-lysine (0.5 mg/mL; Sigma-Aldrich), kept for 3 h, and replaced with neurobasal growth medium containing B27 supplement, 0.5 mM L-glutamax (Sigma-Aldrich), penicillin (100 U/mL), and streptomycin (100 mg/mL). The cells were kept at 37°C in an incubator with 5% CO_2 and 95% air for 3 days before further treatment. Cultures were fed daily with neurobasal growth medium containing B27 supplement.

Four days after plating, DRG neurons were treated with recombinant human GDNF (100 ng/mL, R&D Systems) or vehicle for the indicated time points and then used for biochemical assay. In some experiments, cells were pretreated with anti-GDNF antibody (at the dose of 6, 3, and 1.5 μg/mL, respectively, Abcam), RPI-1 (20 μM, Merck Biosciences), PD98059 (20 μM, Merck Biosciences), PP2 (1 μM, Merck Biosciences), LY294002 (20 μM, Merck Biosciences), or anisomycin (10 μg/mL, Merck Biosciences) for 30 min before GDNF (100 ng/mL) stimulation.

Acute dissociation of DRG neurons was performed as described in our previous reports (Fang et al., 2015; Zheng et al., 2013). Briefly, neurons were isolated from the L4 and L5 DRGs of adult rats and were digested using the same procedure as described for primary cell culture above. The dissociated cells were used for patch-clamp recording within 3 to 8 h of plating.

RNA extraction and RT-qPCR

Total RNA was extracted from the rat L4/L5 DRGs with TRIzol reagent (Life Technologies). Reverse transcription was performed with oligo deoxythymidine (oligo-dT) primers and Moloney murine leukemia virus reverse transcriptase (Promega) according to the manufacturer's protocol. Polymerase chain reaction (PCR) primer sequences are listed in Table S1. Real-time quantitative PCR (RT-qPCR) was performed with GoTaq qPCR Master Mix (Promega) and an ABI 7500 Fast Real-Time PCR Detection System (Applied Biosystems). Briefly, a 20-μL PCR reaction that included 1 μL of complementary DNA, 10 μL of GoTaq qPCR Master Mix, and 0.2 μM of each primer was used and adjusted to the final volume with double distilled H_2O (ddH_2O). β-actin in parallel for each run was used as an internal control. The reactions were set up on the basis of the manufacturer's protocol. PCR conditions were incubation at 95°C for 3 min followed by 40 cycles of thermal cycling (10 s at 95°C, 20 s at 58°C, and 10 s at 72°C). The relative expression ratio of mRNA was quantified via the $2^{-\Delta\Delta CT}$ method.

Western blotting

Cultured DRG neurons or the dissected rat L4/L5 DRGs were immediately homogenized in ice-cold lysis buffer containing 50 mM tris (pH 8.0), 150 mM NaCl, 1% NP-40 (Sigma-Aldrich), 0.5% sodium deoxycholate (Sigma-Aldrich), 0.1% sodium dodecyl sulfate (SDS), 1% protease inhibitor cocktail, and 1% protein phosphatase inhibitor cocktails (Roche, Indianapolis, IN). After being rotated at 4°C for 1 h, the homogenates were centrifuged at 12,000 rpm for 10 min to yield the total protein extract in the supernatant, and the supernatant was analyzed.

For western blot analysis, 40 μg or 60 μg of total protein was loaded dependent on the reactivity of different antibody. However, the amount was the same within one analysis. e.g., for the antibodies of P2X3R, pERK1/2, ERK1/2, and GFRα1, our preliminary study showed that 40 μg total protein is appropriate for the blots, at this amount not only obtained clear blots but also eliminated the overexposed and saturated signals that were observed at the loading of 60 μg total protein. Whereas for the antibodies of pRunx1 and Runx1, which are difficult to obtain obvious blots with the loading of 40 μg total protein, thus 60 μg of total protein was loaded to obtain clear blot signals. The sample containing total amount of protein was denatured and then separated through SDS-polyacrylamide gel electrophoresis (SDS-PAGE) using 10% to 12% separating gels and transferred to a PVDF membrane (Bio-Rad, Hercules, CA). The membranes were blocked with 5% nonfat milk or bovine serum albumin in Tris-buffered saline and Tween [TBST, 20 mM tris-HCl (pH 7.5), 150 mM NaCl, and 0.05% Tween 20] for 60 min at room temperature, and then incubated with the following primary antibodies at 4°C overnight: rabbit anti-rat P2X3R antibody (1:1000, Alomone Labs), rabbit anti-rat pERK1/2 antibody (1:1000, Cell Signaling Technology), rabbit anti-rat ERK1/2 antibody (1:2000, Cell Signaling Technology), rabbit anti-rat pRunx1^{Ser249} (1:500, Cell Signaling Technology), rabbit anti-Runx1 (1:1000, Abcam), rabbit anti-GFRα1 (1:1000, Santa Cruz), mouse anti-β-actin (1:2000, Santa Cruz Biotechnology), or mouse anti-GAPDH (1:2000, Santa Cruz Biotechnology). The blots were washed in TBST and then were incubated in horseradish peroxidase-conjugated secondary antibody (1:2000, goat anti-rabbit/mouse or rabbit anti-goat IgG). Protein bands were visualized using an enhanced chemiluminescence detection kit (Pierce) followed by autoradiography using Hyperfilm MP (Santa Cruz Biotechnology). The band was quantified with a computer-assisted imaging analysis system (ImageJ, NIH).

For the Blots within the same figure, the same samples were used throughout the whole manuscript, i.e., the same samples were used on the same gels for the western blots within the same figure. For the proteins that have approximately the same molecular weight, stripping was used to remove the primary and

secondary antibodies of the former protein on the membrane, and then incubated the antibody of the next protein. Similarly, if three proteins with close molecular weight on the same gel, the stripping would be repeated twice. For the proteins with obviously different molecular weight, we clipped the PVDF membrane at each molecular weight location with the guide of the molecular weight marker after electro-transferring. Then we incubated the corresponding antibody on the membrane, respectively.

At the beginning of the present study, to determine the feasibility of the experimental designs, we performed some *in vitro* experiments mainly on cultured DRG neurons, and GAPDH was used as a housekeeping gene as described in previous studies (Gattenloehner et al., 2007; Kim et al., 2020; Xiang et al., 2008). However, we found that its stability is not as good as we expected, and the alteration of GAPDH expression indeed is found in a variety of cancer types including the breast cancer (Guo et al., 2013). In fact, GAPDH is a key enzyme that catalyzes the redox reaction in the glycolytic pathway and glycolysis is enhanced in several cancer cells (Liu et al., 2017; Zheng, 2012). Elevated expression of GAPDH seems related to cancer development and metastasis (Epner et al., 1993 May 1; Tang et al., 2012). Therefore, we selected β-actin as a housekeeping gene in our later experiments as most researchers used in bone cancer pain studies (Liu et al., 2015; Meng et al., 2015; Zhou et al., 2015).

Enzyme-linked immunosorbent assay

To collect tissues for GDNF content analysis, the animals were rapidly decapitated, and the L4/L5 DRGs was excised and placed into a Petri dish containing dry-ice-cold homogenizing buffer. Then they were homogenized in cold extraction Tris-buffered saline (pH 8.0) containing 1% NP-40, 10% glycerol, 0.5 mM sodium metavanadate, 1 mM phenylmethylsulfonyl fiuoride, 10 mg/mL aprotinin, and 1 mg/mL leupeptin. The lysates were centrifuged for 15 min at 12000 g, and a commercially available enzyme-linked immunosorbent assay (ELISA) kit (Promege, USA) was used to detect GDNF content in the supernatants. This monoclonal antibody shows no cross-reactivity with other neurotrophins (NT-3, NT-4, brain-derived neurotrophic factor or nerve growth factor). GDNF content in the DRGs was normalized to the amount of total protein, which was determined at the same time as the ELISA using a BCA protein assay kit (Pierce, Rockford, IL). Because the solid DRG tissues were obtained and only the weight but not volume could be measured, therefore the GDNF level was expressed in pg/mg total protein rather than pg/mL volume.

Immunofluorescence staining

To prepare DRG tissue samples for immunofluorescence analysis, deeply anesthetized rats were intracardially perfused with 50 mL of 0.1 M phosphate buffer (PB), followed by 500 mL of cold 4% paraformaldehyde [in 0.1MPB (pH 7.4)]. After perfusion, the ipsilateral L4/5 DRG tissues were removed quickly after being fixed for 4 h in the perfusion fixative, and cryoprotected in 30% sucrose [in 0.1 M phosphate-buffered saline (PBS)] overnight at 4°C. Serial frozen DRG sections (10 μm thick) were cut on a cryostat and thaw mounted on gelatin-coated slides for immunostaining processing. For immunostaining, the tissues were washed three times in PBS for 5 min each and blocked in 10% donkey serum (in 0.1 M PBS) with 0.3% Triton X-100 for 1 h at room temperature. Then, tissues were incubated with the respective primary antibody in PBS at 4°C overnight, which includes guinea pig anti-P2X3R (1:200, Novus) and rabbit anti-mouse Runx1 (1:200, Abcam). Then, after three washes in PBS, the tissues were incubated with the following appropriate secondary antibodies at room temperature for 1 h: Cy3 conjugated donkey anti-mouse IgG (1:500, Jackson ImmunoResearch), FITC conjugated donkey anti-rabbit IgG (1:500, Jackson ImmunoResearch), 647 conjugated donkey anti-guinea pig IgG (1:500, Jackson ImmunoResearch). In some experiments, the tissues were counterstained with the nuclear marker DAPI (100 ng/mL) carrying blue fluorescence for 10 min at room temperature. Visualization of fluorescence signal was performed by confocal microscopy at excitation wavelengths of 488 nm (green), 543 nm (red), and 405 nm (blue). At least four fields per section were analyzed to establish reproducibility.

Electrophysiology

Whole-cell patch-clamp recordings from acutely dissociated or primary cultured DRG neurons were performed at room temperature using an EPC-10 amplifier and Patch-Master software (HEKA, Freiburg, Germany). Patch pipettes were pulled from borosilicate glass capillaries with a tip resistance of 5 to 8 MΩ when filled with internal solution containing 140 mM K-aspartate, 20 mM NaCl, 10 mM ethylene glycol tetraacetic acid (EGTA), and 5 mM 4-(2-hydroxyethyl) piperazine-1-ethanesulfonic acid (HEPES), adjusted to pH 7.3 with potassium hydroxide (KOH). The external solution contained 155 mM NaCl, 5 mM KCl, 2 mM $CaCl_2$, 1 mM $MgCl_2$, 10 mM HEPES, and 12 mM glucose, adjusted to pH 7.4 with NaOH (Liu et al., 2013). Drugs

were prepared in the external solution and delivered by an RSC 200 fast-flow delivery system (Biologic Science Instruments, Grenoble, France). Membrane currents and voltage were measured with pipette and membrane capacitance cancellation, filtered at 2 kHz, and digitized at 10 kHz. Resting membrane potential was measured immediately after rupture of the cell membrane in whole-cell patch mode.

Under voltage-clamp recording, cells were clamped at −60 mV, and series resistance was compensated 70 to 90%. The membrane capacitance was read from the amplifier by Patch-Master software (HEKA) for determining the size of cells and calculating the current density. The agonist-evoked P2X3R currents were measured by application of α,β-meATP (20 μM for 3 s). Under current-clamp recording, the cells were held at 0 pA, and the firing threshold of DRG neurons was first measured by a series of 100-ms depolarizing current injection in 5-pA steps from 0 pA to elicit the first AP. To further examine the firing properties of neurons, a large depolarizing current (1000 ms, 2-fold AP threshold) was delivered to elicit the cell generating sufficient firing. In this study, only small-diameter DRG neurons were selected for patch-clamp recording. Somata of the small-diameter DRG neurons were classified by their diameters (≤26 μm) and Cm (≤45 pF) as described in previous reports (Huang and Song, 2008; Vilceanu et al., 2010; Zheng et al., 2012). Origin software 8.5 (OriginLab Corporation, Northampton, MA) was used for data analysis.

In the patch-clamp recording experiments, after a cell (DRG neuron) was clamped, the neuronal excitability was first examined under the current-clamp mode. Then we switched to the voltage-clamp mode to record the α,β-meATP-induced P2X3R currents. At this recording mode, the α,β-meATP was administered to the cell by a perfusion system, the Bio-Logic's Rapid Solution Changer (RSC-200) (https://www.biologic.net/products/rsc200/). The operation of perfusion usually results in the disruption of the giga-seal for the clamped cells. Therefore, we cannot make success for recording P2X3R current in each clamped cell under voltage-clamp mode. As a result, the numbers of recorded cells in the voltage-clamp mode are usually less than those in the current-clamp mode.

QUANTIFICATION AND STATISTICAL ANALYSIS

Statistical analyses were performed with GraphPad Prism 8.0 for Windows (GraphPad Software, La Jolla, CA). All quantitative biochemical data and histologic staining are representative of at least three independent biological replicates. Shapiro-Wilk tests were used to assess normality in the distribution (Gaussian distribution) for each group, and only the data were normally distributed and variances were similar between groups to be compared were subjected to parametric statistical tests. Two-tailed unpaired Student's *t* test was used for the comparison of the mean values between two groups. One-way analysis of variance (ANOVA) with Tukey's or Dunnett's *post hoc* test as indicated in the text, or two-way ANOVA (treatment and time factors) with Sidak's *post hoc* test was used for multiple comparison. All data are reported as mean ± SEM, and differences with $p < 0.05$ were considered statistically significant. *$p < 0.05$; **$p < 0.01$; ***$p < 0.001$; ns., not significant. All statistical data are presented in Table S3, and all source data are presented in Table S4.